FY 2016 Annual Report and

8th Quarter Research Performance Progress Report

Project Title:	Chemical control of fluid flow and contaminant release in shale microfractures
Project Period:	10/01/14 – 09/30/16
Reporting Period:	10/01/15 – 09/30/16
Submission Date:	11/30/2016
Recipient:	SLAC National Accelerator Laboratory
Recipient DUNS #:	00-921-4214
Address:	2575 Sand Hill Road, MS 69
	Menlo Park, CA 94025
Website (if available)	www-ssrl.slac.stanford.edu
Award Number:	FWP 100211
Awarding Agency:	NETL

Principal Investigator:	Dr. John Bargar
	Senior Staff Scientist
	SLAC National Accelerator Laboratory
	Phone: 650-926-4949
	Email: bargar@slac.stanford.edu
Co-Principal Investigators:	Dr. Gordon E. Brown, Jr.
	Dr. Kate Maher
NETL Project Manager:	David Cercone

TABLE OF CONTENTS

1. EXECUTIVE SUMMARY

Stimulation of unconventional source rock (shale) using hydraulic fracturing recovers less than 30% of natural gas and less than 5% of oil, while consuming large volumes of water and producing similarly large volumes of flowback and produced water. Improving efficiency is imperative because of its impact on ultimate hydrocarbon recovery, but also because it provides a route to reducing water demand and problems associated with storing, treating, and disposing flowback and produced water. Formation damage, *i.e.* the reduction in the permeability of source rock caused by injected fluids, is believed to be an underlying cause of reduced hydrocarbon recovery. The introduction of fluids into shales initiates myriad geochemical reactions, including mineral dissolution, oxidation of organic and inorganic species, release of metals, and precipitation of solids [*e.g.* iron or aluminum (oxyhydr-)oxides, carbonates, and sulfates]. For example, oxygen in fracture fluid oxidizes pyrite (abundant in shales), leading to precipitation of iron (oxyhydr-)oxides that clog fractures and pore space, potentially blocking flow of hydrocarbons and fluids. These chemical reactions also release metal and radionuclide contaminants such as uranium, lead, nickel into flowback water, creating the potential for human exposure to radioactive elements and heavy metal contaminants. In spite of the high reactivity of fracture fluid with shale, there is a general lack of fundamental information about fracture fluid-rock geochemical processes in shale. Yet, improved knowledge and control over shale-fluid reactions could be used to reduce formation damage, improve production efficiency, improve overall water usage, and reduce risk of contamination of clean surface and ground water.

The objectives of this research program were to: (1) uncover key chemical processes occurring during shale-fluid reactions, and (2) develop detailed quantitative models that can be used to understand the geochemical behavior of hydraulically stimulated reservoirs, to predict permeability changes, and to mitigate contaminant behavior. To accomplish these objectives, we characterized the products (dissolved and solid phases) formed by the reaction of fracture fluids with shale minerals and kerogen and identified precipitates at spatial scales down to that of individual precipitate grains (*i.e.* down to the nm level).

Impact: Knowledge developed by this project is helping geochemists and engineers to understand how shale formation damage occurs and to predict the long-term geochemical evolution of hydraulically stimulated shale systems. Ultimately, this knowledge will help improve hydrocarbon recovery and, decrease contamination risk, and improve improve utilization of water resources.

The period under review comprises the second year of an initial 18-month project, which was extended to 24 months years in February 2016 without expanding the project cost. This document also serves as the 8th quarter report for the project. During the first three quarters of the year (quarters 5-7 of the project), we focused on performing measurements and analyzing data that was required to write manuscripts. During the 8th quarter, our efforts were directed largely towards writing and submitting manuscripts. In addition, however, we also completed sequential extractions of uranium from shales and analyzed the resulting liquid and solid samples (tasks 4.10 and 4.11). We also completed additional kerogen-fracture fluid reaction experiments and data analyses (task 3.7) that were needed to write an additional manuscript.

As shown in **Figure 1**, dissolved oxygen in fracture fluid is expected to oxidize pyrite (abundant in shales), releasing Fe^{2+}, which can lead to the precipitation of Fe(III)-(oxyhydr-)oxides. Depending on the pH-buffering capacity of the shale, different morphologies and compositions of Fe(III)-bearing phases can precipitate, including poorly crystalline ferrihydrite and highly crystalline hematite. Additionally, the potential enhancement of Fe oxidation and precipitation at both low and circum-neutral pH by organics added to the fracture fluid or by bitumen (labile non-hydrocarbon organics) is being investigated.

A fundamental challenge posed by shale-fracture fluid reactions is that changes to the porosity of the shale are complex. In certain situations, reactions of shales with fracture fluids can cause mineral dissolution, which increases porosity, whereas in other situations, occlusion of pores can occur through the formation of mineral precipitates. Even submicron-thick accumulations of mineral coatings have the potential to cause "formation damage", *i.e.* reduce permeability and attenuate discharge of hydrocarbons from fractures and across fracture walls. This proposal responded to the urgent need to understand the basic geochemical reactions that occur when fracture fluids react with fractured shale. Such knowledge is prerequisite to improving hydrocarbon production efficiency and minimizing environmental impact.

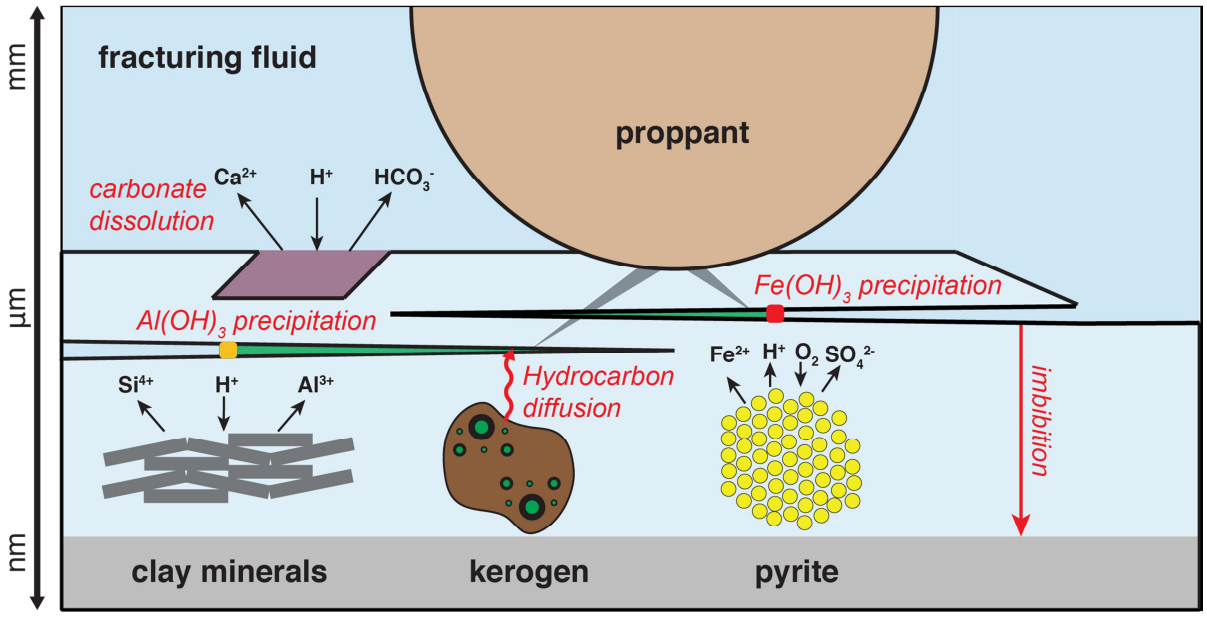

Figure 1. Conceptual model of alteration processes occurring during hydraulic fracturing operations. Fracture fluid-shale reactions can drive secondary porosity generation, iron redox cycling, precipitation of fracture-clogging minerals, and release of contaminants such as uranium.

Scientific and technical accomplishments:

- 3 manuscripts in review or published, with additional manuscripts in preparation
- Featured lead article in the NETL Fall 2015 E&P Newsletter
- 23 presentations (7 invited) at (inter)national scientific/industrial venues (Appendix A)
- Completion of all project milestones

Four key scientific discoveries have emerged from this work:

1) **Carbonate minerals are a master control on geochemical processes.** Carbonate mineral content profoundly affects the geochemical response of shale to acidic fracture fluid. Hydraulic stimulation initiated by injection of acid drives dissolution of carbonate, pyrite, and silicate. Rapid carbonate dissolution buffers low-pH fluids, consuming acidity and reducing the overall chemical attack on other minerals. Consequently, carbonate-rich and carbonate-poor rocks respond differently to fracture fluids. Our work shows that carbonate-rich shales rapidly neutralize acidic fracture fluids, leading to lower contaminant release but much more rapid oxidation and scale precipitation. In contrast, fracture fluids interacting with carbonate-poor, siliceous shales have lower pH values, release larger amounts of uranium and heavy metal contaminants, but result in relatively slow Fe(II) oxidation and dramatically reduced scale precipitation. These findings lead to specific models for chemical-mechanical formation damage, which we are now linking to matrix permeability evolution and long-term production efficiency.

2) **Shale organics dramatically accelerate precipitation of iron scale.** Oxygen (and oxidants such as persulfate) in fracture fluid causes pyrite to oxidize, releasing Fe(II) that can also be oxidized and precipitate as insoluble Fe(III) (oxy-)hydroxides (goethite, hematite, and ferrihydrite) that clogs pores and pore necks. Our research shows that this process is strongly accelerated in the presence of bitumen leached from shale by fracture fluid, as well as by organic fluid additives. These findings indicate that iron control is more difficult to achieve than previously recognized and emphasize the importance of avoiding conditions that cause iron dissolution from Fe-bearing minerals such as pyrite. Moreover, this discovery implies that shale organics may be involved in other precipitation reactions, such as barite scale precipitation. Our new project is taking direct aim at testing this hypothesis through a series of experiments designed to evaluate the impacts of shale organics on mineral precipitation.

3) **Fracture fluid stimulates and then mitigates uranium release.** Our research shows that reaction of shales with acidic fracture fluid causes large-scale release of uranium. Moreover, kerogen in particular was found to release large amounts of metals, including iron, nickel, and lead. However, after initial reaction, dissolved uranium and metal concentrations decline over time spans of weeks to months. Our geochemical models show that uranium and metals are reabsorbed onto precipitating scale, most likely iron minerals. These findings imply that uranium and metal release can be controlled through manipulation of iron chemistry.

4) **Reactivity of kerogen.** Kerogenic pores are believed to be important to oil and gas transport. Fracture fluid was found to have minimal chemical impacts on kerogen. These results suggest that fracture fluid probably is not a significant source of damage to organic pore networks during hydraulic fracturing.

2. GOALS AND OBJECTIVES

The objectives of this research program were to characterize products (dissolved and solid phases) formed by the reaction of fracture fluids with shale minerals and kerogen and to assess the compositions and morphologies of coatings and aperture-clogging precipitates at spatial scales down to that of individual fracture coatings (*i.e.* down to the nm level). In addition, we have characterized the impact of fracture fluid-rock interactions on uranium mobilization from shales as a proxy for toxic redox-active trace metal and radionuclide mobilization.

During the second year of the project, we have completed all key milestones, and observed novel and sometimes unexpected phenomena. We have submitted two manuscripts at this juncture (Task 2, and a separate manuscript combining results from Tasks 4, 5 and 6) with significant progress on an additional manuscript (Task 3). We also expect to publish further manuscripts over the next year based on experimental results obtained during this project.

The project is subdivided into a management task (Task 1) and five research tasks. The experimental approach is designed to systematically probe fracture fluid reactions with the primary constituents of shales, including Fe(II) (Task 2), and kerogen (Task 3). These results are being used to understand the products formed when whole shales react with fracture fluids (Task 4). Uranium release following reaction of shales with fracture fluids is being assessed in Task 5. A geochemical fluid-shale reaction model is being developed during Task 6 to improve quantitative prediction of shale-fluid reaction products under varied shale compositions and chemical conditions.

3. TECHNICAL HIGHLIGHTS, RESULTS, AND DISCUSSION

Summary of accomplishments in year 2. Important progress included the following:

Task 2

1. Completion of Fe(II)/bitumen reactors at various O_2 concentrations and identification of Fe(III)-bearing precipitates
2. Analysis of synchrotron-based XRF maps for unreacted and reacted shale samples
3. Analysis of bulk Fe K-edge EXAFS spectra of unreacted and reacted shale samples
4. Submission of manuscript

Task 3

5. Completion of all experiments necessary to write a manuscript
6. Progress on writing of manuscript for this task

Task 4

7. Completion of all experiments necessary to write a manuscript
8. Submission of manuscript for Task 4, which also contains results from Task 6.

Task 5

9. Completion of synchrotron-based spectroscopic analyses of uranium in shale
10. Completion of sequential chemical extractions for U on all 4 shale types (unreacted and reacted with hydraulic fracturing solution.

Task 6

11. Finalization of model parameters and successful modeling of experimental data.
12. Submission of manuscript for Task 6, which also contains results from Task 4.

Details of task progress.

Task 1. Project management. See sections 4 (risk analysis), 5 (milestone status), and 6 (schedule status).

Task 2. Fe(II) and bitumen reactions with fracture-fluid

In early experiments, the release of Fe(II) from shales and subsequent precipitation of Fe(III)-(oxyhydr-)oxides were found to be highly dependent on shale type and the presence of organics in fracture fluid. This variable behavior could not be predicted from existing literature data using our geochemical model. Knowledge of the underlying source of this complex behavior is required to understand precipitation of "yellow boy", *i.e.* mixtures of Fe(III)-(oxyhydr-)oxides formed following oxidation of pyrite in shales during their exposure to fracture fluids. Task 2 was subsequently focused on understanding the behavior of Fe(III) derived from the reaction of pyrite with fracture fluid, with an emphasis on the influence of bitumen on this reaction. The use of synchrotron-based x-ray absorption spectroscopy (XAS), however, has shown that a significant amount of the Fe contained in the shale samples examined here is bound directly to carbon in kerogen. Additionally, XAS data also indicate that the inorganic forms of Fe (primarily Fe-sulfides) are the most reactive species while Fe bound to organics is relatively stable. By combining XAS with micro x-ray fluorescence (μ-XRF) mapping, the types of precipitates containing Fe that formed for the different shales samples studied were determined. As described below, the differences in iron precipitates and their distributions caused by differences in the mineralogy of the four types of shales we examined are potentially very important in controlling the distribution of fracture-clogging Fe(III)-(oxyhydr-)oxide precipitates.

Progress in the quarters 5-7. Data analysis and experiments for Task 2 were completed during the 7th quarter. Bitumen was isolated from Marcellus and Green River shales using a toluene-methanol extraction procedure. In a series of subsequent experiments, isolated bitumen was redissolved in aqueous solutions of varying composition, including HCl only, fracture fluid without HCl, and fracture fluid with HCl. The total concentration of bitumen was set at 40 ppm. The initial pH for the reactors was set at either pH = 2.0 or pH = 7.1 to determine the effect of pH on Fe(II) oxidation in the presence of bitumen. De-oxygenated solutions of $FeCl_2$ were added to reach final Fe(II) concentrations of 40 ppm. Samples were incubated at 80^{o}C and sacrificed at 0,

2, 5, 8, 17, 24, and 48 hours. Iron (II) and total iron concentrations were determined using Ferrozine and hydroxylamine hydrochloride (for total iron), and UV/Vis spectrophotometry.

Progress in the 8th quarter. The focus of the 8th quarter was on preparing the manuscript. The initial draft of the manuscript was completed and revised. This manuscript has been submitted to *Energy & Fuels*.

Results. As an extension of the Fe(II)/bitumen work outlined in the previous Annual Report it was necessary to determine the effect on dissolved O_2 on the ability of bitumen to override the pH inhibition effect on Fe(II) oxidation. It was found that regardless of the system pH, when O_2 was not included in the Fe(II)/bitumen reactors there was no detectable Fe(II) oxidation over the span of one week of incubation time. This result indicates that O_2 is necessary for the oxidation of Fe(II) followed by the precipitation of Fe(III)-bearing phases. The precipitates produced in the Fe(II)/bitumen reactors that were open to atmosphere were analyzed using XRD to determine the crystalline phases produced during the 48 hour incubation period. For the low pH system (pH = 2.0), 2-line ferrihydrite was produced during the first 48 hours. In the higher pH (pH = 7.1) system, the Fe(III)-bearing phase detected in the first 48 hours was goethite. When both pH reactors were incubated for a total of 3 weeks the Fe(III)-bearing phases produced in 48 hours converted to hematite. The initial Fe(III)-bearing phases produced in these different pH bitumen reactors at 48 hours mirror that of the shale reactors in which speciation was varied based on pH of the system (see below).

Table 1. Task 2 objectives for quarters 5-8. Objectives completed in quarter 8 are indicated with bolded text.

Goal	Status
Preliminary Fe(II) oxidation experiments with bitumen	Complete
Fe(II) oxidation experiments with bitumen and varying dissolved O_2	Complete
Fe(II)/bitumen reactor experiments without O_2	Complete
Analysis of synchrotron-based μ-XRF mapping of unreacted and reacted shale (multi-element and Fe specific) collected in December 2015	Complete
Analysis of Fe(III)-bearing precipitates from Fe(II)/bitumen reactors with abundant O_2 after 48 hour and 3 week incubations	Complete
Scanning Transmission X-ray Microscopy (STXM) analysis of Marcellus and Green River bitumen	Complete
Identification of Fe(III)-bearing precipitates from Fe(II)-bitumen reactors	Complete
Analysis of bulk Fe K-edge EXAFS data collected in April 2016	Complete
Manuscript writing	**Complete**

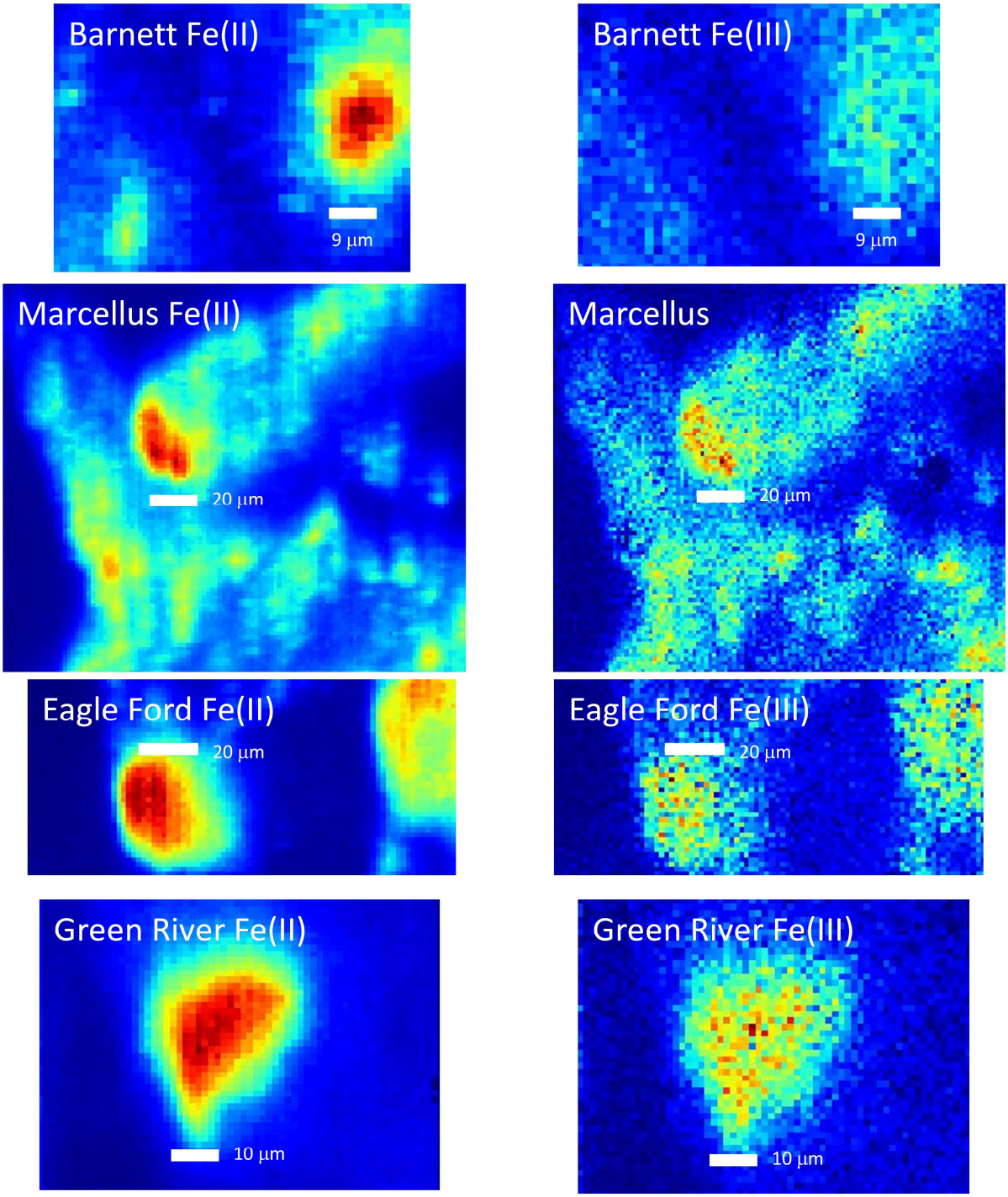

Figure 2: Iron K-edge synchrotron μ-XRF imaging of Fe(II) (left column) and Fe(III) (right column) in the unreacted oil/gas shale sand-sized samples. Pyrite is the dominant Fe(II)-bearing phase for Barnett, Eagle Ford, and Marcellus. Fe(III)-rich regions are almost exclusively magnetite. For the Green River sample, fits to spectra (not shown) indicate that the Fe(II)/Fe(III) zone in the figure is a mixture of pyrrhotite and goethite.

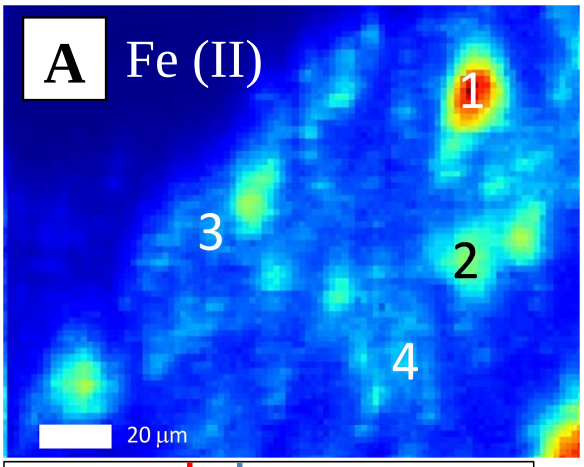

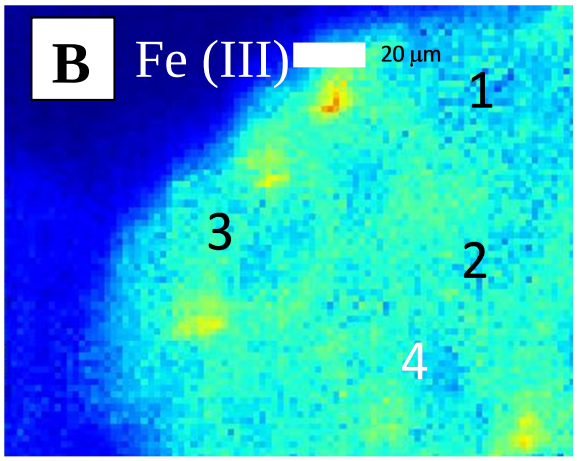

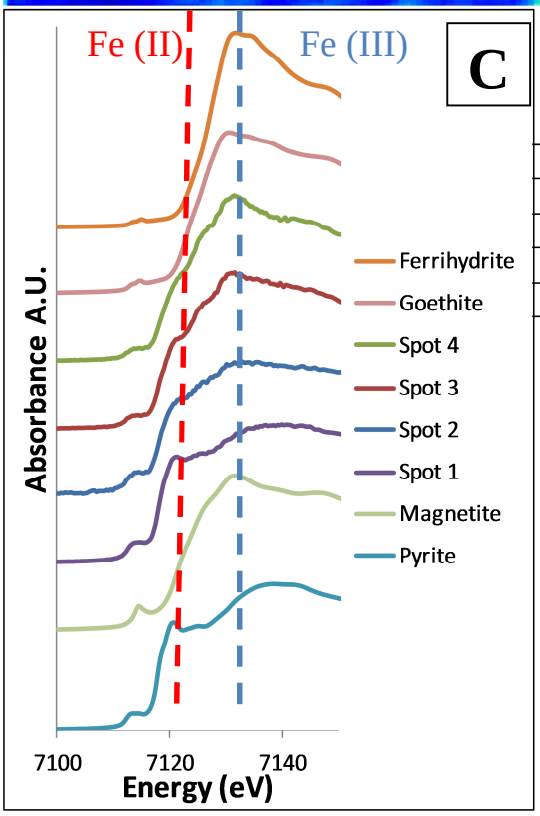

D

	Pyrite	Magnetite	Ferrihydrite	Goethite	R-Value
Spot 1	86 %	14 %	N.D.	N.D.	0.000373
Spot 2	46 %	54 %	N.D.	N.D.	0.000396
Spot 3	38 %	14 %	48 %	N.D.	0.000416
Spot 4	27 %	16 %	16 %	41 %	0.000382

Figure 3: **A**. Fe(II) and **B**. Fe(III) µ-XRF maps for a sand particle from the 3-week reacted Marcellus Shale. **C.** Fe K-edge µ-XANES spectra of 4 selected positions from the above µ-XRF images. **D.** Linear combination fitting results of the 4 selected positions showing shift from Fe(II) to Fe(III) dominated regions. N.D. stands for "Non-detect".

The µ-XRF mapping resulted in significant results. Mapping of the Fe(II) and Fe(III) for the four shales selected for this work (Marcellus, Barnett, Eagle Ford, and Green River) was done prior to reaction to determine whether outcrop samples (Marcellus and Green River) were highly weathered compared to samples taken at depth (Barnett and Eagle Ford). The µ-XRF maps (**Figure 2**) coupled with micro-x-ray absorption near edge structure (µ-XANES) spectroscopy indicate that all four samples contain a small amount of Fe(III) in the form of magnetite. Surprisingly, the only sample that contained goethite in the unreacted sample was the Barnett shale taken at a depth of 2613 m. These results show that if samples from outcrop samples are

taken several centimeters from the rock surface, weathering is of little concern and the samples can be directly compared with those taken at depth. The speciation of Fe(II) hot spots as seen in **Figure 2** is almost exclusively pyrite (> 95% of the Fe(II) phases) in Marcellus, Barnett, and Eagle Ford, with trace amounts of siderite and magnetite. The Green River shale differed in the Fe(II) speciation with pyrrhothite, a sulfur-deficient Fe-sulfide, being the dominant Fe(II)-bearing phase with small isolated grains of ilmenite also being present in the rock.

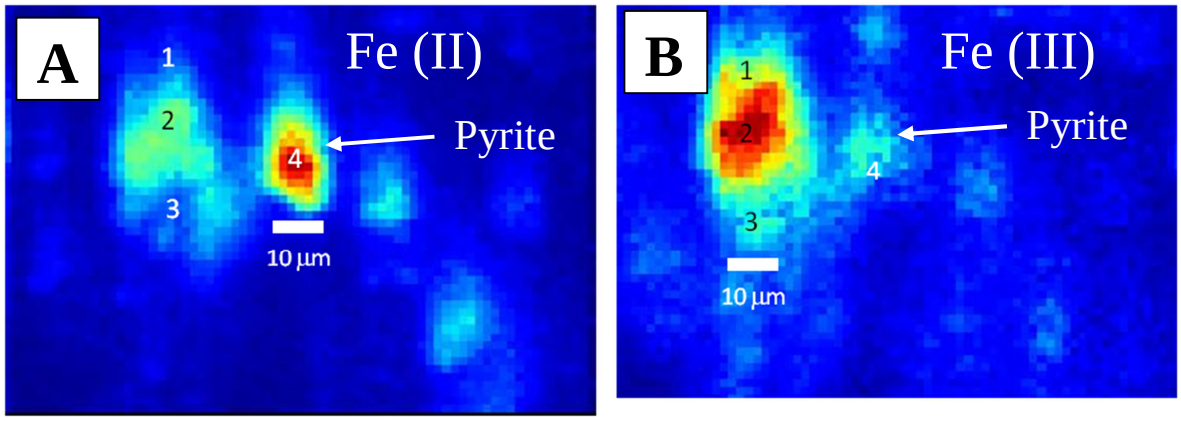

C

	Pyrite	Pyrrhotite	Magnetite	Hematite	R-Value
Spot 1	19 %	N.D.	37 %	45 %	0.002858
Spot 2	12 %	N.D.	37 %	51 %	0.003642
Spot 3	41 %	N.D.	36 %	23 %	0.000165
Spot 4	54 %	34 %	12 %	N.D.	0.000677

Figure 4: A. Fe(II) and **B**. Fe(III) µ-XRF maps for a sand-sized particle from the 3-week reacted Eagle Ford Shale. **C.** Linear combination fitting results of the 4 selected positions showing shift from Fe(II) to Fe(III) dominated regions with the presence of significant quantities of hematite. N.D. stands for "Non-detect".

The post-reaction analysis of the shale samples by µ-XRF mapping and µ-XANES indicate that the buffering capacity of the rocks play a large role on the morphology and phase of Fe formed. In systems with low pH buffering capacity, Marcellus and Barnett, the Fe(III)-bearing precipitates form diffuse coatings that are on the surfaces and matrix of the sand-sized shale samples (**Figure 3**) as opposed to discreet mineral crystals as seen in the Eagle Ford samples (**Figure 4**). As seen in **Figure 3** for the Marcellus shale, there is a significant shift in Fe speciation away from pyrite framboids with the production of ferrihydrite (closer to framboids) and a mixture of ferrihydrite and goethite farther away from the pyrite framboids. The continued presence of magnetite, as well as the increase in amount of magnetite in certain regions, indicate that as O_2 in the system is consumed, Fe(III) in solution will react with the Fe(II) in the system to produce magnetite. The Fe solution data from these reactors (**Figure 5**) show that some of the Fe released into solution can remain as Fe(II) for weeks prior to oxidizing and precipitating. The long residence time for Fe(II) in solution, coupled with the diffuse and widespread Fe(III)-bearing precipitates in the low pH buffering systems, suggests that Fe(II) released in these systems can travel long distances in solution prior to oxidation and precipitation which could

severely impact permeability in kerogen, pore necks, piping, etc., far away from the Fe source. In contrast, in systems with high pH buffering capacity, such as Eagle Ford, Fe(III)-bearing precipitates form as discreet crystals as opposed to more diffuse surface coatings (**Figure 4**). As shown in **Figure 4**, a discreet crystal that is a mixture of hematite and magnetite formed near the pyrite grain. In addition, **Figure 4** shows a newly formed Fe(II)/Fe(III) crystal 10's of μm in size. Such crystals have a high potential for pore occlusion in the shale matrix. Unlike the low pH buffering systems, the chances of Fe(III)-bearing precipitates impacting permeability at distances far away from the Fe source is small in the high pH buffering systems. Also of note, the pyrite crystal in the Eagle Ford sample does show leaching of S from the mineral as suggested by the presence of S-deficient pyrrhotite.

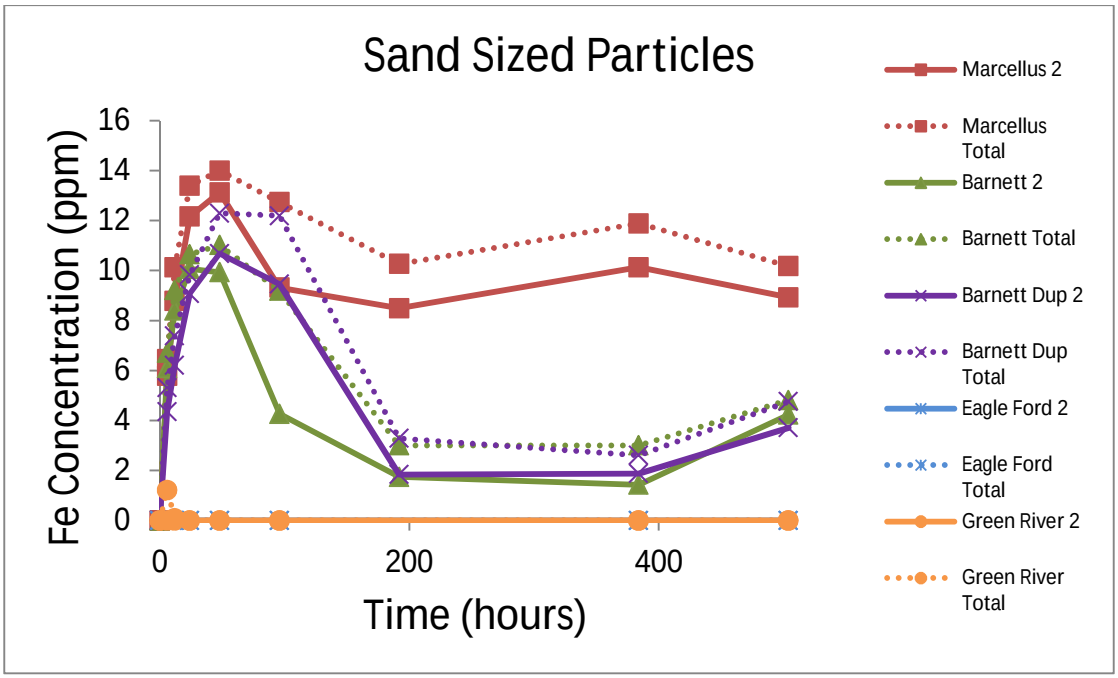

Figure 5: Iron release curve from sand-sized shale samples. The number "2" denotes Fe(II) concentrations while "Total" denotes total Fe concentrations in solution. Error in triplicate samples is < 8%.

The bulk EXAFS show significantly different results compared to the μ-XRF mapping coupled with μ-XANES spectroscopy. This is because bulk EXAFS spectroscopy probes the Fe-bearing species over a large spatial region (8mm x 1mm) as opposed to μ-XANES spectroscopy, which probes a region ~1μm x 1μm. As seen from the unreacted Marcellus shale EXAFS data (**Figure 6)**, the bulk of the EXAFS signal is from a mixture of pyrite and an unknown Fe-bearing phase that generated an oscillation at k = 4. All EXAFS spectra except for one contain this unknown oscillation that does not correspond to any of the inorganic Fe phases (Fe(II) or Fe(III)) in our reference library (> 50 reference EXAFS spectra). Due to the prominence of this feature, shell-by-shell fitting of the 3-week reacted Green River shale was completed using single scattering pathways corresponding to pyrite with the inclusion of Fe bound to X (X corresponds to N, C, O, P, B, CN, Cl, NO_3, PO_4, S, SO_3, or SO_4). The shell-by-shell fit indicates that the unknown oscillation is due to an Fe-C bond at a distance of 2.11 Å (**Figure 7**). An attempt to use

other ligands often found in organic material (N, O, S, etc.) at the distance of 2.11 Å in the fit was unsuccessful, which confirms that an Fe-C pair correlation is responsible for this oscillation in the EXAFS spectra at ~ k = 4 Å^{-1}. A schematic of the Fe-S, Fe-Fe, and Fe-C interactions for pyrite and ferrocene is shown in **Figure 7**. In order to do proper linear combination fitting (LCF) of the shale Fe K-edge EXAFS spectra, the EXAFS spectrum of a natural sample of Fe(II) bound to humic material with an Fe-C distance of 2.09 Å was used in conjunction with the EXAFS spectra of inorganic Fe reference compounds. Results of the LCF indicates that in almost all samples, except Green River shale samples, pyrite is the dominant Fe-bearing phase present (**Figure 7**). Similar to that seen in **Figure 7**, contributions from Fe-organics are present in every EXAFS spectra except for that of the unreacted Eagle Ford shale. The small variation in the proportion of Fe-Organics in every shale sample suggests that the Fe contained in the organic fraction is more stable than the inorganic Fe phases.

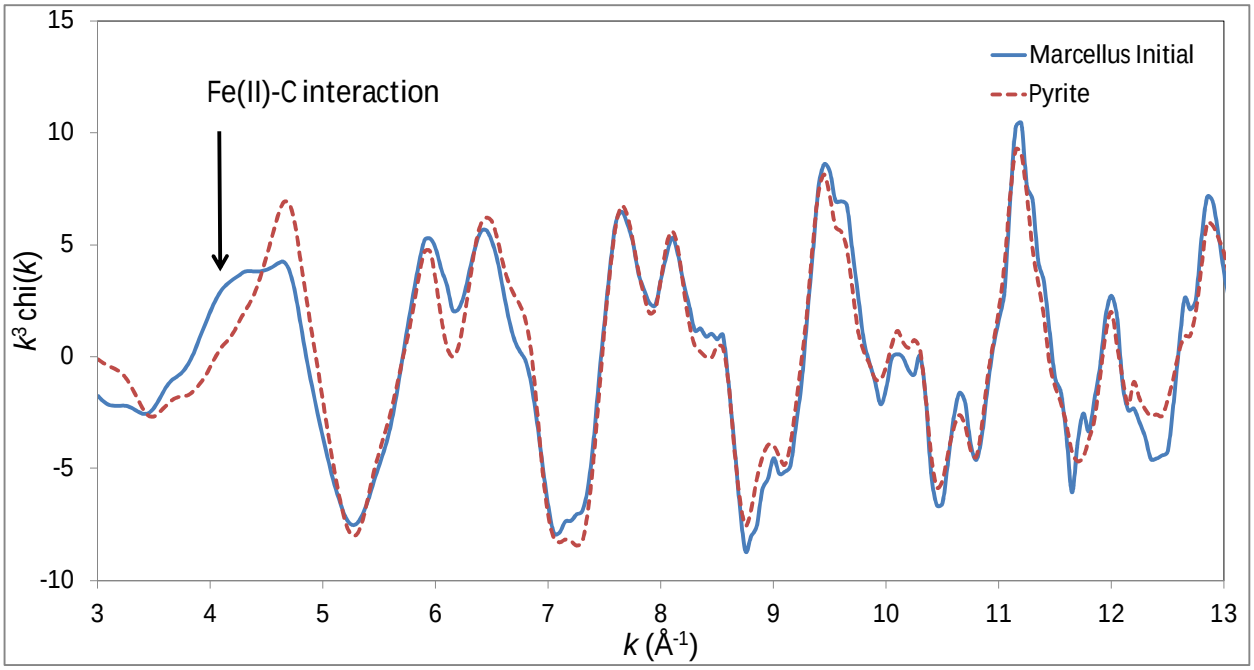

Figure 6: Bulk Fe K-edge EXAFS of the Marcellus shale prior to reaction with hydraulic fracturing fluid. The dashed line is a pyrite reference compound illustrating that the majority of the features are due to pyrite. The feature at k = 4 is not consistent with any inorganic Fe compound in the reference library. Shell-by-shell fitting of the data indicates that the feature at k = 4 is consistent with an Fe(II)/C interaction at 2.11 Å.

To determine if the Fe-Organics EXAFS signal is from Fe in the bitumen or in kerogen, scanning transmission x-ray microscopy (STXM) on isolated kerogen and bitumen samples was completed at the Advanced Light Source at Lawrence Berkeley Lab. STXM results for the isolated bitumen showed no detectable Fe while the kerogen samples showed pyrite particles in the kerogen matrix along with other unidentifiable Fe-bearing regions. Because of the lack of Fe detected in the isolated bitumen and the presence of Fe-rich regions in the kerogen not associated with pyrite, it is assumed that the Fe-Organics feature in the EXAFS spectra is from Fe in the kerogen. The bulk EXAFS results show that the Barnett shale had the least amount of change for the Fe while both the Eagle Ford and Green River (high carbonate) shales had the most alteration

of the shale. The EXAFS data for the inorganic Fe phases for Marcellus shale are consistent with the μ-XANES data described above, where the majority of the Fe(III)-bearing phases is in the form of ferrihydrite, a common Fe(III)-hydroxide nanomineral. Results for Eagle Ford shale are also consistent with μ-XANES of the more crystalline Fe(III)-bearing phases geothite and hematite, suggesting that one or both of these crystalline phases is present. The dominant Fe speciation in the shale reactors is also consistent with the speciation of the Fe precipitates in the Fe(II)/bitumen reactors that were incubated for 48 hours, indicating that in the short-term (< 1 year), the pH of the system influences the Fe(III)-bearing phase produced.

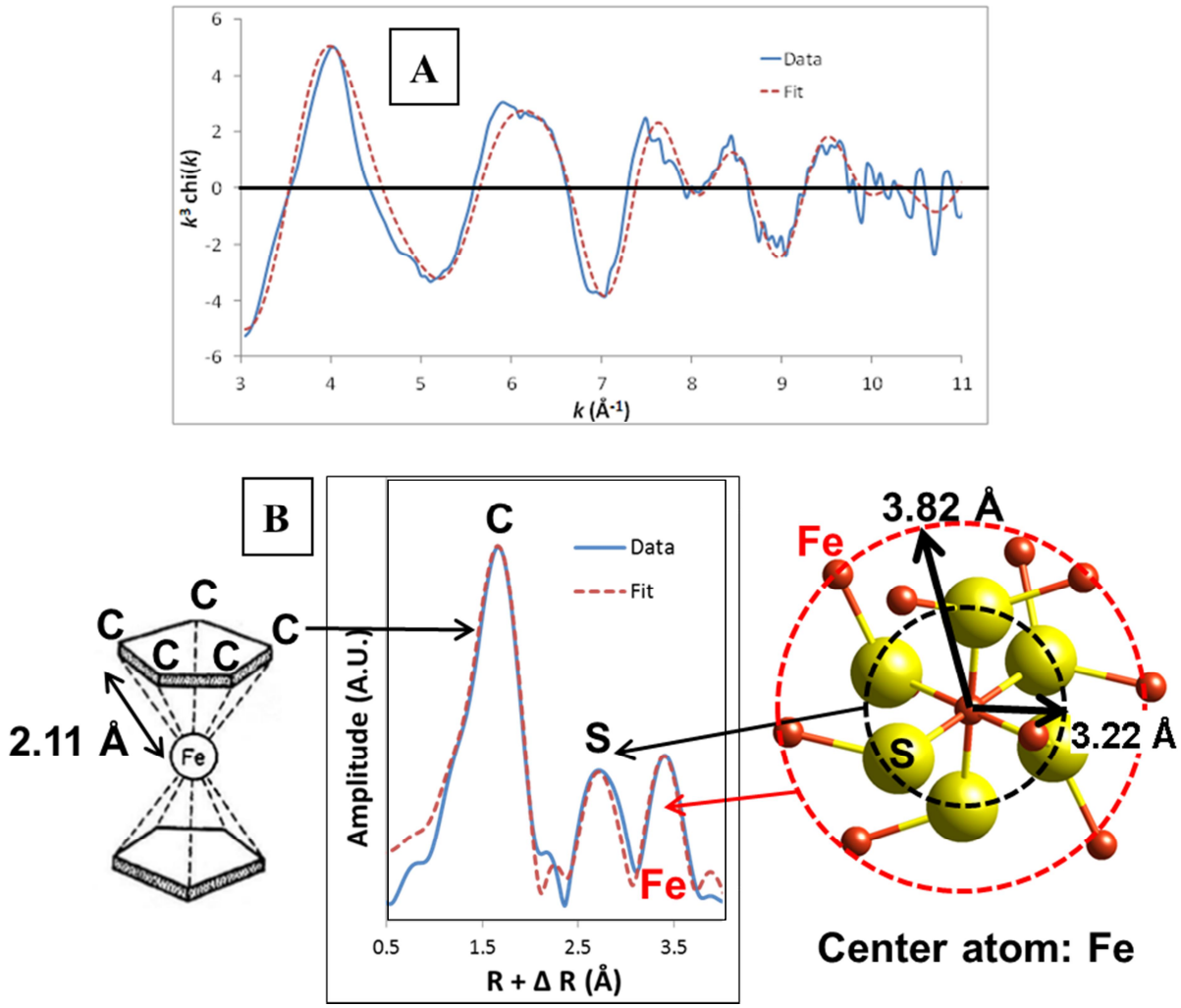

Figure 7: **A.** Bulk Fe K-edge EXAFS spectrum from Marcellus shale prior to reaction with hydraulic fracturing fluid (blue line). The red dashed line is the spectrum from pyrite. The overall similarity of the spectra indicates that pyrite is dominant. However, the feature at k = 4 is not consistent with inorganic Fe. Shell-by-shell fitting of the data indicates that the feature at k = 4 is consistent with the presence of neighboring C atoms at 2.11 Å. This is illustrated in the Fourier transform of the EXAFS spectrum (**B**). The blue data in the Fourier transform (FT) plot are from the shale sample, but the red dashed curve shows the fit to the spectrum assuming a shell of C atoms at a Fe-C separation of 2.11 Å. As shown by the illustration of the ferrocene molecule to the left, the 2.11 Å distance is typical of Fe-C bonds.

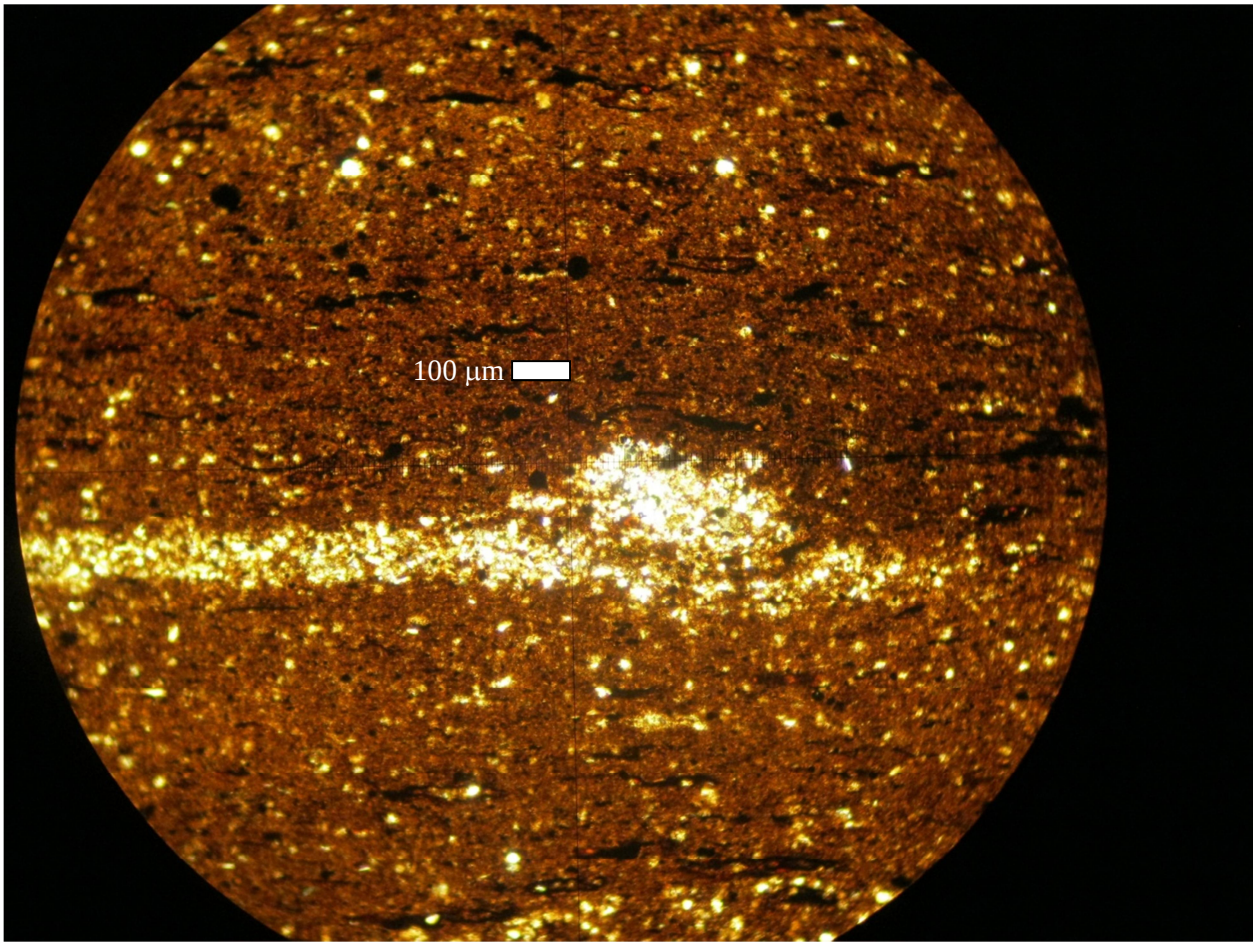

Figure 8: Petrographic thin section under plain polarized light perpendicular to bedding of unreacted Marcellus shale. The white box illustrates the typical morphology and high abundance of kerogen in the shale while the green box indicates typical morphology of pyrite.

Due to the complexity of the Green River Fe K-edge EXAFS spectra, the data were fit with a combination of EXAFS spectra of unreacted shale, 3-Week reacted shale, and 3-Week reacted kerogen. The 3-Week reacted kerogen was selected because there is a detectable difference between the EXAFS spectra of the unreacted and 3-Week reacted Green River kerogens. Based on the LCF of the Green River EXAFS data, inorganic Fe is more reactive than the Fe/kerogen component. Additionally, there is very little difference between the EXAFS spectra of the 3-Month and 6-Month reacted Green River shales.

The discrepancy between the μ-XANES and the bulk EXAFS results is a matter of scale. As seen in a petrographic thin section of the Marcellus shale cut perpendicular to bedding (**Figure 8**), there is high heterogeneity in these shale samples not seen on the hand specimen scale. Since the μ-XANES data were collected on regions that had the highest Fe fluorescence in the XRF maps, the regions selected for μ-XANES analysis were not the kerogen regions but the pyrite crystals scattered throughout the shale.

Manuscript Plans. We currently have the manuscript for this task completed. The manuscript title is: Importance of pH, Oxygen, and Bitumen on the Oxidation and Precipitation of Iron during Hydraulic Fracturing of Oil/Gas Shales. This has been submitted to *Energy & Fuels*.

Deliverables. In addition to the manuscript, this work resulted in one poster presentation at the Stanford Synchrotron Radiation Lightsource 2016 User's meeting (Jew *et al*.; Appendix A), one poster at the 2016 Stanford Natural Gas Initiative Meeting, one poster was presented at the American Geophysical Union 2015 Fall Meeting (Jew *et al*.; Appendix A), and one talk scheduled for the 2016 American Geophysical Union Fall Meeting in December.

Task 3. Kerogen-fracture fluid interactions

Kerogen is an integral part of oil- and gas-shale systems, comprising up to 40% of the volume of some major gas-producing shale plays (Passey *et al*., 2010). It is the source of economically important hydrocarbons and has complex associations with minerals in the shales, such as pyrite and clays (Salmon *et al*., 2000). It is also mechanically incompetent and thus may contribute to fracture development. Kerogenic pores are also considered to be major conduits for oil and gas within shales (Thomas *et al*., 1990). Quantifying the role of kerogen in mineral-fluid interactions is thus critical to optimizing and predicting oil and gas recovery and quantifying environmental impact. For example, the wettability of kerogen is important in controlling hydrocarbon migration and fluid flow in shales. As kerogen's wettability is determined by its surface functional group chemistry, alteration of the material could impact transport of both hydrocarbons and fracture fluid. Although it is known that kerogen is largely hydrophobic, modeling studies have suggested that fracturing fluids may imbibe into organic pores due to capillary effects (Hu *et al*., 2014), allowing for fluid-organic matter reactions. However, there has been no research on how hydraulic fracture fluids interact chemically with kerogen. The large majority of research concerning chemical reaction of kerogen has instead centered on functional group evolution during thermal maturity, which occurs gradually over much longer timeframes (i.e. Durand, 1980; Craddock *et al*., 2015). Additionally, kerogen has been shown to contain elevated concentrations of redox-sensitive metal(loids) (Filby *et al.*, 1994). The ability of kerogen to act as a contaminant source or sink in the context of hydraulic fracturing is unknown, and the potential for contaminants to be released or desorb from kerogen has been relatively unexplored. We hypothesized that these metal(loids) have the potential to be mobilized after contact with hydraulic fracture fluid or other solutions, but that the contribution from kerogen would be small relative to the contribution from mineral matter.

In this task, kerogen was isolated from the Marcellus and Green River shales in order to determine reactions that occur when this material is exposed to hydraulic fracture fluid. The two kerogens represent end-member compositions: the Marcellus represents a thermally mature kerogen while Green River is relatively thermally immature. The two kerogens are also classified as different Types; Types of kerogen differ in their functional group composition based on source organisms and depositional environment. The Marcellus shale was chosen because of its economic importance, while the Green River as a useful contrast based on its thermal immaturity and classification as a Type I rather than Type II kerogen. It was also chosen for the abundance of kerogen, which was required to evaluate kerogen isolation and characterization methods.

Progress in the Quarters 5-7. Marcellus kerogen was successfully isolated, and short and intermediate-term reactors were completed with this material (2 weeks and 3 months). For these reactors, the amounts of kerogen and solution were decreased (keeping the fluid:solid the same). The short-term timeframe was therefore shortened from 3 weeks to 2 weeks. This was done because of sample limitation and the desire to limit the decrease in the fluid:solid ratio with excessive sampling. Based on the results from the Green River kerogen reactors, a 6-month Marcellus kerogen reactor was not deemed necessary.

Solutions from all reactors were analyzed by the ferrozine method for Fe^{2+} and Fe^{3+} concentrations, ion chromatography (IC), inductively coupled plasma mass spectrometry and optical emission spectroscopy (ICP-MS and ICP-OES), and TOC/TN. Solids from all reactors were analyzed by X-ray diffraction (XRD), X-ray fluorescence (XRF), Fourier transform infrared spectroscopy (FTIR), Elemental Analysis (EA), scanning electron microscopy (SEM), and X-ray absorption spectroscopy (Fe K-edge). Gases from reactors were analyzed by gas chromatography (GC) for CO_2 and O_2 concentrations.

Table 2. Task 3 objectives for quarters 5-8. Objectives completed in quarter 8 are indicated with bolded text.

Goal	Status
Short-term (3 week) reaction of kerogen with hydraulic fracture fluid	Complete
Extraction of kerogen from Marcellus Shale	Complete
Ferrozine assay (Fe^{2+} and Fe_{tot} concentrations)	Complete
Dumas combustion measurements	Complete
ICP-OES and ICP-MS for total metal concentrations	Complete
XRF analysis of post-reaction kerogen	Complete
XRD analysis of post-reaction kerogen	Complete
SEM analysis of post-reaction kerogen	Complete
GC analysis of gas samples	**Complete**
FTIR analysis of post-reaction kerogen	**Complete**
Additional kerogen-fracture fluid reactions required for manuscript	**Complete**
Initiate writing manuscript draft	**Compete**

Progress in Quarter 8.

Additional kerogen experiments were conducted to complete the data set for manuscript preparation. Experiments containing Green River and Marcellus kerogen and solutions lacking the organic fracture fluid chemicals (water and hydrochloric acid only) were reacted for 2 weeks. In addition, aliquots of the Green River and Marcellus kerogens were placed in a gamma-irradiator overnight for sterilization and then used in 2 week reactors with fracture fluid. These control experiments are needed to discount the possibility of alteration by microbial activity.

Quarter 8 also included additional analyses and a refinement of the fitting method for FTIR results. Finally, manuscript writing was initiated.

Results.

Metal(loid) behavior. XRF analyses of both kerogens demonstrates that they are enriched in metal(loids) (**Figure 9**). Green River is significantly more enriched in many elements relative to the Marcellus. This observation is in accordance with the scientific literature, which notes that trace element are often preferentially enriched in shale organic matter (Leventhanl, 1993). Solution data indicate substantial release of many of these elements to solution during reaction with fracturing fluid. However, because there is no reliable method for removing sulfide minerals from kerogen without damaging the organics, the isolated kerogen materials used in experimental reactors include pyrite, pyrrhothite, and other trace sulfide species. Of note, trends among the fracture fluid, water with hydrochloric acid, and sterile reactors are generally indistinguishable. This indicates that the mobilization trends for metals within kerogen and associated pyrite is unaffected by the organic fracture fluid additives or any potential microbial activity within the experimental reactors.

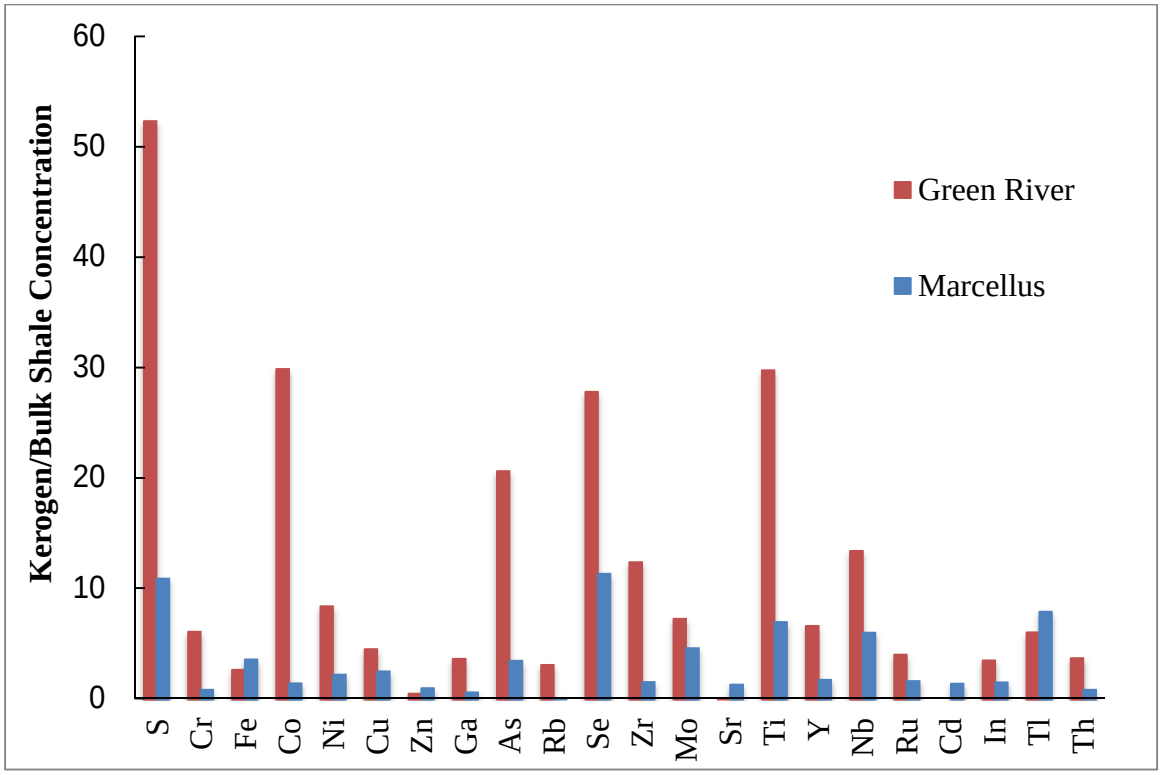

Figure 9: Relative enrichments of elements in the Green River and Marcellus isolated kerogens, as calculated by XRF measurements. Enrichments were calculated by normalizing concentrations in the isolated kerogen by the concentrations in the respective bulk shale.

The elements mobilized in the Marcellus kerogen in significant concentrations are those that should be dominantly associated with pyrite (Fe, S, Co, Ni, Pb). It seems unlikely, therefore, that desorption or decomplexation from kerogen is a substantial source of metal(loids) in the

Marcellus shale. Because there is a higher pyrite content in the Marcellus kerogen, the release of these elements is much greater in the Marcellus than the Green River.

A notable difference between metal release and apparent pyrite dissolution can be observed when comparing Fe:S ratios in solution. For example, Fe:S ratios in Green River reactor solutions are significantly higher than in the corresponding Marcellus reactors and cannot be explained by the dissolution of iron sulfide minerals alone (**Figure 10**). This is confirmed by Fe K-edge EXAFS of Green River kerogen and shale (**Figure 7**), where least-squares fitting indicates a significant portion of the iron is directly bound to carbon. This likely represents iron sorbed to the more reactive functional groups such as carboxylic groups that are often present in immature kerogen but are absent in thermally mature organic matter. Fe:S ratios are also highest in the first 100 hours of reaction, suggesting that desorption of iron is a relatively rapid process. Recognizing the timescale of contaminant mobilization in this way is important to understanding produced water chemistry.

It is difficult to analyze other trace metals in a similar method by creating ratios to Fe or S, since the trace element content of the iron sulfide minerals remaining in the two kerogens in unknown. However, examining trace element data reveals some potential insights. Co, Ni, and Pb (common impurities within pyrite) concentrations are much greater in Marcellus solutions. However, Zn and Cu show different behavior (**Figure 11**). Zn concentrations are similar in Marcellus and Green River reactors, and Cu concentrations are much higher in Green River reactors. However, it does appear that there may be some Cu re-precipitation in the Marcellus reactors. Although Zn and Cu are potential trace elements found in sulfide minerals, their anomalously high concentrations in Green River solutions indicate they may also be partially sourced from kerogen. There may be a propensity for divalent metals to sorb to more immature kerogen (Fe, Zn, Cu, among others) and be mobilized after reaction with oxidized fluids.

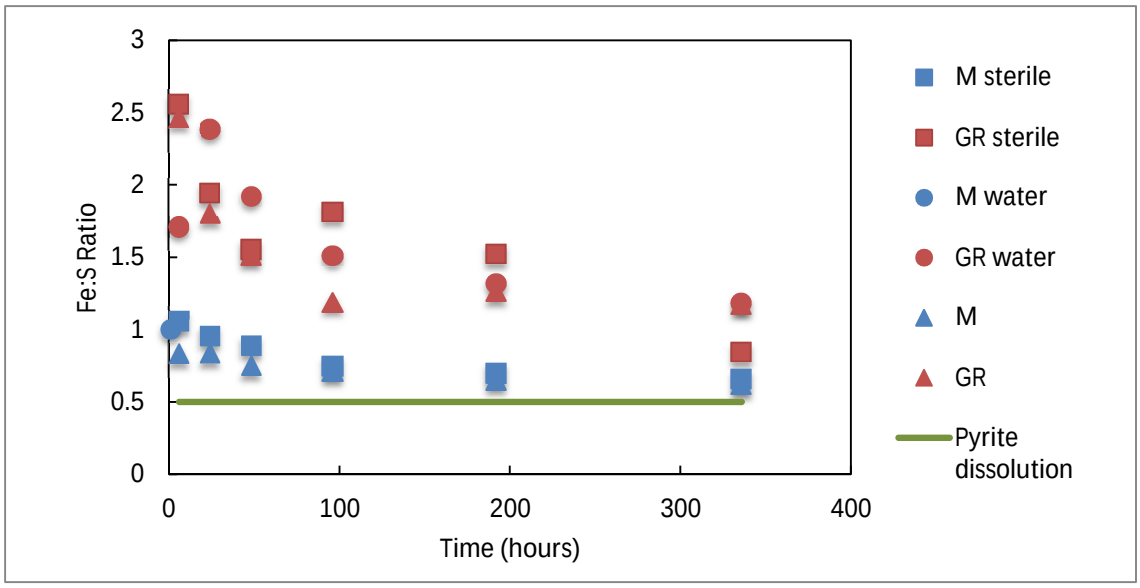

Figure 10: Fe:S ratios in solution. Total Fe and S concentrations were measured by ICP-OES. The orange line represents the stoichiometry that would expected solely due to the dissolution of pyrite. The dissolution of pyrrhotite or marcasite would instead result in a Fe:S ratio of 1.

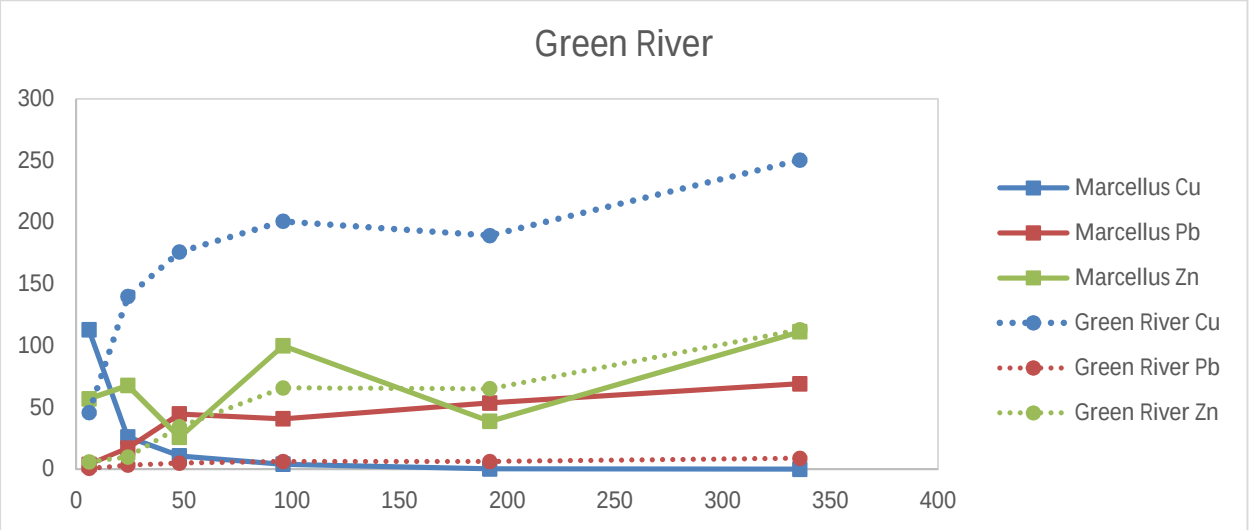

Figure 11: Trace element concentrations in solution during kerogen experiments, as measured by ICP-MS. The Pb data is representative of other trace element data (i.e. Ni, Co). Zn and Cu represent two notable exceptions to the trends. There are no significant differences in concentrations for sterile and water/hydrochloric acid reactors among the same kerogen type.

Overall, the trace metal results are significant since total dissolved solids, and therefore contaminants of interest in produced waters, have traditionally been thought to originate solely from mineral-fluid reactions (Chapman *et al*., 2012). Results from these experiments suggest that in addition to mineral dissolution/precipitation, more thermally immature kerogen may impact the compositions of produced waters. They also demonstrate that sulfide minerals hosted in organic matter may be an important source of contaminants of interest.

Kerogen alteration. In the second year, the understanding of potential changes to kerogen composition with reaction evolved significantly. The addition of the Marcellus kerogen experiments, an expanded sample set, and an improved FTIR fitting method allowed important conclusions to be drawn about kerogen-fracture fluid interactions.

A careful analysis of Fourier Transform infrared spectroscopy (FTIR) data of unreacted and reacted kerogen was completed using the IgorPro software for peak analysis (**Figure 12**). Peak assignments were made based on several literature sources, including Rouxhet *et al*. (1980), Lin and Ritz (1993), and Parikh *et al*. (2014). Previously, portions of interest in the spectra were identified and fit in sections of 900-1800 cm^{-1} and 2600-3400 cm^{-1}. In an effort to resolve uncertainties, the method was further refined by fitting only the sections 1200-1500 cm^{-1} and 1500-1800 cm^{-1}. These two sections capture the most important peaks: a region of aliphatic C-H bend which captures a peak representing CH_2 and CH_3 and a peak representing only CH_3, and the aromatic C=C stretch next to the C=O stretch indicative of carbonyl. Because of the influence of broad peaks indicative of mineral matter, the best fits are achieved by applying a cubic background to the 1200-1500 cm^{-1} section and a constant background to the 1500-1800 cm^{-1} section. The ratios of these relative peak intensities can then be compared to reveal information about the importance of different functional groups. Aliphatic chain length, an important parameter in measuring the extent of kerogen maturation or reaction, is investigated by comparing the relative influence of CH_3 vs. CH_2. Similarly, potential oxidation of kerogen can be

monitored by observing the carbonyl:aromatic peak ratios, since oxygenated functional groups such as carbonyl would increase with reaction. Results show that there is not significant variation between reacted and unreacted kerogen samples. A 1-20% variation in ratios was observed for duplicate analyses of the same samples, indicating either measurement error or kerogen heterogeneity. Any variation in reacted and unreacted samples falls within this region of uncertainty. Given the absence of clear trends for FTIR analyses, it is impossible to identify any alteration to organic functional groups. While minor alteration is possible, apparent heterogeneity and uncertainties in analyses prevent this level of scrutiny. In order to further clarify, samples have been shipped to GeoMark for RockEval pyrolysis to determine O and H content.

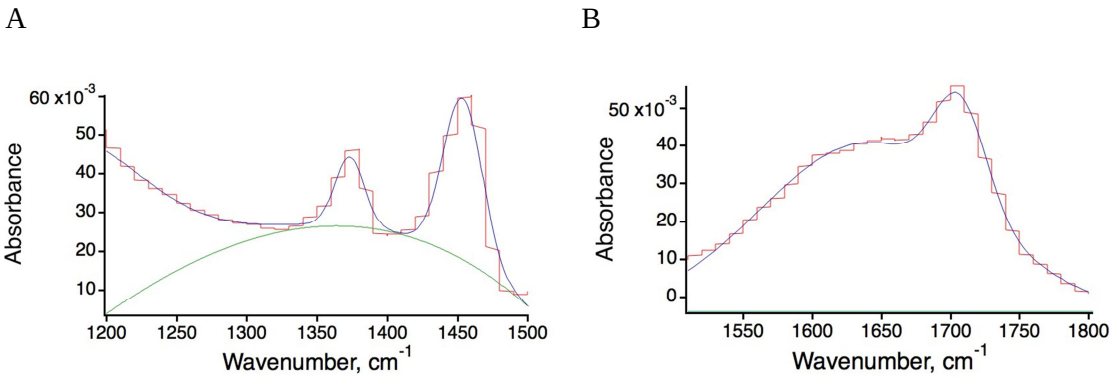

Figure 12: Example fits of FTIR spectra, from Green River kerogen reacted with fracture fluid for 2 weeks. In each panel, the actual spectrum is shown in red, fits are overlain in blue, and background is shown as green. A) Region of 1200-1500 cm^{-1} B) Region of 1500-1800 cm^{-1}.

Potential alteration of organic matter degradation can be tracked by mass balance. Previous C and N measurements showed a modest loss of C in both the Green River and Marcellus and loss of N within the Green River. However, analyzing a larger sample set (including sterile and water with hydrochloric acid samples and re-analyzing previous samples) reveals a spread in C and N values that is not consistent. For example, some reacted samples exhibit higher C or N than unreacted samples, and C:N ratios are not consistent. This level of variation is not observed when analyzing a shale standard, suggesting these discrepancies are not due to measurement error. This information instead suggests that the isolated kerogen product is highly heterogeneous, which is in accordance with the documented heterogeneous nature of kerogen. Additionally, solutions from the water and hydrochloric acid only reactors were analyzed for the most common organic acids that were potentially leached using ion chromatography. Solutions from fracture fluid reactors cannot be analyzed due to major interferences from the organic additives. The results show that solutions contain less than 0.1 mM acetate and no detectable propionate or butyrate, indicating minimal solubilization.

While it initially appeared that minor alteration occurred after reaction with fracture fluid, an expanded sample set and refined FTIR fitting method revealed no apparent changes in carbon content or relative functional group abundances. The updated conceptual understanding of kerogen's limited reactivity with fracture fluid is important for evaluating hydrocarbon and fracture fluid flow in hydraulic fracturing conditions. Because of the apparent structural and compositional integrity of kerogen when exposed to fracture fluid, there is an experimental basis to believe kerogenic pores will maintain their properties even as substantial geochemical reactions occur within the reservoir.

Manuscript Plans. A manuscript is in progress which details the successful isolation of high purity kerogen (both Green River and Marcellus), its potential for metal release to solution and implications for contaminant mobility, and the limited tendency for organic carbon alteration.

Deliverables. In addition to the manuscript, this work resulted in one poster presentation at the American Geophysical Union 2015 Fall Meeting (Dustin *et al*) and one poster presentation at the Stanford Synchrotron Radiation Lightsource 2016 User's meeting (Dustin *et al*.; Appendix A).

References.

Chapman, E.C., Capo, R.C., Stewart, B.W., Kirby, C.S., Hammack, R.W., Schroeder, K.T. and Edenborn, H.M. Geochemical and strontium isotope characterization of produced waters from Marcellus shale natural gas extraction. *Env. Sci. Technol*. **2012**. 46, 3545-3553.

Craddock, P.R., Le Doan, T.V., Bake, K., Polyakov, M., Charsky, A. and Pomerantz, A.E. Evolution of kerogen and bitumen during thermal maturation during semi-open pyrolysis investigated by infrared spectroscopy. *Ener. Fuel.* **2015.** 29, 2197-2210.

Durand, B. Sedimentary organic matter and kerogen. Definition and quantitative importance of kerogen. In: Durand (Ed.), Kerogen, Insoluble Organic Matter from Sedimentary Rocks. **1980**. Editions Technip, Paris, pp. 13-34.

Filby, R.H. Origin and nature of trace element species in crude oils, bitumens, and kerogens: implications for correlation and other geochemical studies. *Geological Society*, London. **1994**. 78, 203-219.

Hu, Y., Devegowda, D. and Sigal, R.F. Impact of maturity on kerogen pore wettability: a modeling study. SPE Annual Technical Conference and Exhibition. **2014.** 27-29.

Leventhal, J. Metals in Black Shales. In: Engel and Macko (Eds.), Organic Geochemistry Principles and Applications. **1993.** Plenum Press, New York and London. Pp. 581-591.

Lin, R. and Ritz, G.P. Reflectance FT-IR microspectroscopy of fossil algae contained in organic-rich shales. *Appl. Spectrosc.* **1993**. 47, 265-271.

Marynowski, L., Kurkiewicz, S., Rakocinski, M.Simoneit, B.R.T. Effects of weathering on organic matter: I. Changes in molecular composition of extractable organic compounds caused by paleoweathering of a Lower Carboniferous (Tournaisian) marine black shale. *Chem. Geol.* **2011.** 285, 144-156.

Parikh, S.J., Goyne, K.W., Margenot, A.J., Mukome, F.N.D. and Calderon, F.J. Soil chemical insights provided by vibrational spectroscopy. In: Sparks (Ed.), Advances in Agronomy. **2014.** Academic Press, New York. Pp. 1-112.

Passey, Q.R., Bohacs, K., Esch, W.L., Klimentidis, R. and Sinha, S. From oil-prone source rock to gas-producing shale reservoir – geologic and petrophysical characterization of unconventional shale-gas reservoirs. *SPE*. **2010**.

Rouxhet, P.G., Robin, P.L. and Nicaise, G. Characterization of kerogens and of their evolution by infrared spectroscopy. In: Durand (Ed.), Kerogen, Insoluble Organic Matter from Sedimentary Rocks. **1980**. Editions Technip, Paris, pp. 13-34.

Salmon, V., Derenne, S., Lallier-Verges, E., Largeau, C. and Beaudoin, B. Protection of organic matter by mineral matrix in a Cenomanian black shale. *Org. Geochem.* **2000.** 31, 463-474.

Thomas, M.M. and Clouse, J.A. Primary migration by diffusion through kerogen: II. Hydrocarbon diffusivities in kerogen. *Geochim. Cosmochim. Acta.* **1990.** 54, 2781-2792.

Task 4. Whole shale-fracture fluid interaction

This module investigates the impact of fracture fluids on bulk shale samples with emphasis on studying alteration of shale surfaces and coating development as a function of shale composition. Economically important shales from different geological environments representing a wide range of clay, carbonate, and kerogen contents were reacted with fracture fluid in batch reactors at reservoir-representative temperature: Marcellus, Eagle Ford, Barnett, and Green River. Changes in both fluid and solid composition were tracked to gauge reaction progress and inform geochemical models.

Progress in quarters 5-7. The bulk of the experimental work for this task was largely completed in year 1. Important activities conducted in quarters 5 – 7 were required to complete the study and write the manuscript. These activities included completing short-term reactors with limited headspace, run under conditions similar to those outlined in the previous Annual Report and selected to best assess experimental reproducibility over a large range of experimental conditions. In addition, we completed analyses of aqueous and solid-phase samples from the experiments using methods detailed in **Table 3**. Completion of these activities positioned us to begin writing a manuscript, which includes modeling results in Task 6.

Progress in quarter 8. The focus of the 8th quarter was preparing the manuscript that uses data from Tasks 4 and 5 to inform model development (Task 6). The initial draft of the manuscript was completed and revised. This manuscript has been submitted to *Applied Geochemistry*.

Table 3. Task 4 objectives for quarters 5-8. Objectives completed in quarter 8 are indicated with bolded text.

Goal	Status
Complete short-term reactions with O_2-limited headspace	Complete
Analysis of aqueous chemical data with ICP-OES, ICP-MS, and TOC	Complete
Synchrotron-based XRF microprobe mapping	Complete
Analysis of synchrotron-based XRF microprobe mapping data	Complete
Characterize reacted solids using XRD, SEM, FTIR, BET, and EDS	Complete
Re-run of reactors to assess reproducibility	Complete
Analysis of aqueous and solid materials from reactor re-runs	Complete
Draft of manuscript	Complete
Submit manuscript	**Complete**

Results. The re-run of the reactors was completed and showed similar trends in both metal release and porosity changes that were outlined in the previous Annual Report.

Manuscript plans. As noted above, a manuscript that contains results from Tasks 4, 5 and 6 was recently submitted *Applied Geochemistry*.

Deliverables. In addition to the submitted manuscript, this work resulted in one poster presentation at the Stanford Synchrotron Radiation Lightsource 2016 User's meeting (Harrison *et al*.) and one at the American Geophysical Union 2015 Fall Meeting (Joe-Wong *et al*.).

Task 5: Uranium mobilization

Oxygen present in fracture fluids is expected to oxidize relatively insoluble U^{4+} to U^{6+}, which is relatively soluble and mobile in water. Thus, oxidation of shale has the potential to mobilize uranium. The purpose of this task is to examine uranium speciation and release from shales in response to reaction with fracture fluids. Selective chemical extractions and synchrotron-x-ray spectroscopic studies were performed on unreacted and fracture fluid-reacted shale samples. The objective of these chemical extractions is to identify the mineral hosts for uranium in the initial materials and to reconcile observed trends in U release with reaction rates of specific minerals, in order to evaluate the source of uranium released in solution.

Progress in quarters 5-7. Early in the year, the speciation (oxidation state) of uranium in shales was measured using synchrotron-based x-ray spectroscopy. Uranium concentrations in solutions from our Task 4 experiments were analyzed and modeled. Thin sections for uranium radiography were prepared and irradiated. Finally, a protocol of chemical extractions was developed to assess the chemical reactivity uranium in the shales through a series of tests conducted on Marcellus shale. The procedure comprised 6 steps, each being more aggressive than the preceding step and each targeted toward the following specific uranium fractions:

(i) Water-extractable uranium (extractant: ultrapure water)
(ii) Ion-exchangeable uranium (extractant: 1 molar ammonium acetate)
(iii) Carbonate-hosted uranium (extractant: sodium acetate)
(iv) Metal oxide- and phosphate-hosted uranium (extractant: 0.04 molar hydrochloride in 25% nitric acid)
(v) Organic matter- and sulfide-hosted uranium (extractant: 30% hydrogen peroxide)
(vi) Silicate-bound uranium (extractant: 50% hydrofluoric acid)

This extraction procedure was then initiated on unreacted and fracture fluid reacted samples for Marcellus shale (outcrop sample), Green River shale (outcrop sample) and Barnett shale (core sample) samples. Shales were ground to ~250 μm by mortar and pestle. Fracture fluid was prepared less than 48h prior to reaction and the concentrated hydrochloric acid was added just before reaction. The reaction with the fracture fluid lasted 3 weeks at 80°C. During the extraction procedure, the supernatant was recovered using a needle and syringe. Between each extraction step, the samples were washed with Millipore water.

Progress in the 8th quarter. Selective chemical extractions were completed in the 8th quarter. Aqueous supernatants and washing waters were analyzed for uranium concentrations on a Thermo Scientific XSERIES 2 ICP-MS. Bulk shale samples were analyzed with X-ray fluorescence (XRF). Scanning electron microscopy (SEM) was used to measure the grain size of the ground powder and to understand the geometry of the ground shale. The samples (bulk and

residues from the extractions) were analyzed for mineralogical composition on a Rigaku powder X-ray diffractometer (XRD).

Table 4. Task 5 objectives for quarters 5-8. Quarter 8 objectives are indicated with bolded text.

Goal	Status
Analysis of U speciation using synchrotron-based x-ray spectroscopy	Complete
Analysis of U concentrations from fluid-shale reactions using ICP-MS	Complete
Preparation of thin sections for uranium radiography	Complete
Activation of thin sections for uranium radiography	Complete
Sequential chemical extractions of uranium from shale samples	**Complete**
Characterization of uranium samples and solution data from extractions	**Complete**

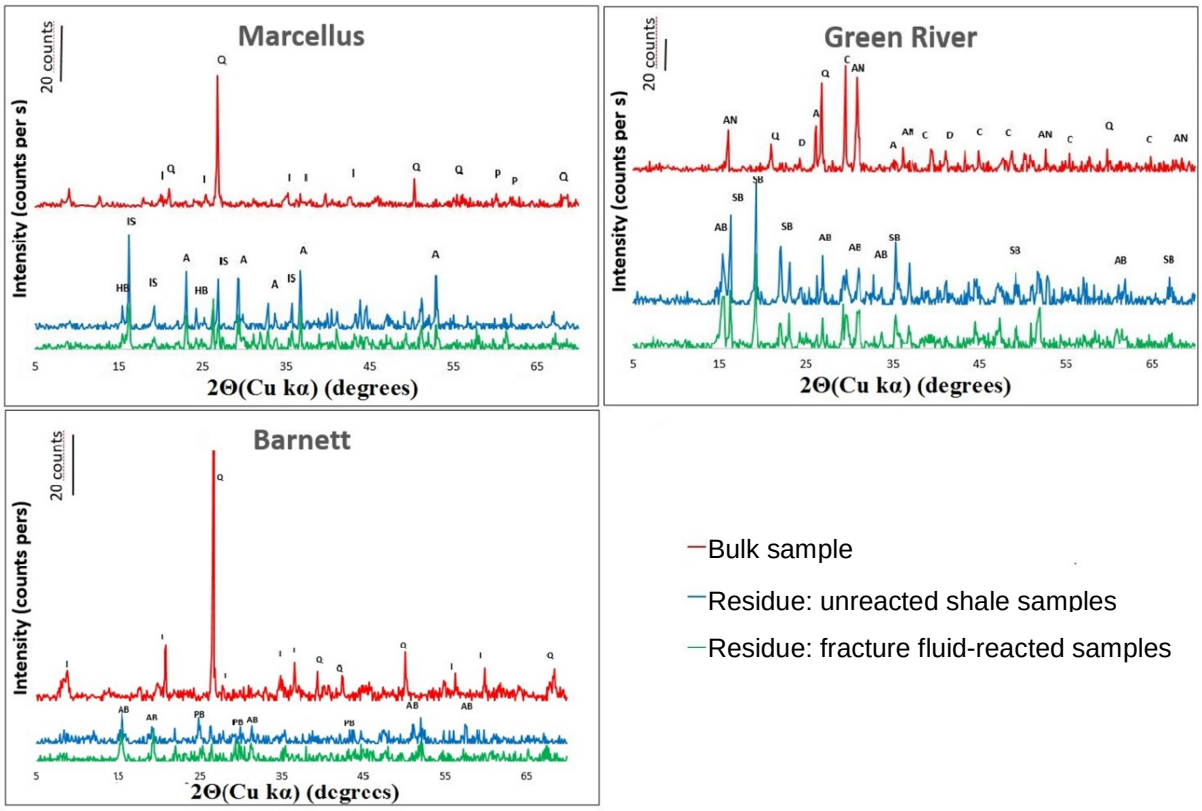

Figure 13 – X-ray diffractograms of bulk samples and the residues for unreacted shale and reacted shales. Are noted the peaks that can be attributed for the bulk sample (Q quartz, I illite, P pyrite, C calcite, D dolomite, AN analcime, A albite) and for the residues (AB aluminum borate, PB potassium borate, HB hydrogen borate, IS iron sulfate, A albite, SB sodium borate). Vertical scale bar is 20 counts.

Results. The analyzed XRD diffractograms of the bulk samples and the extraction residues from the unreacted shale and the reacted shale (shales that were reacted with fracture fluids prior to the chemical extractions) are reported for each shale in **Figure 13**. Only the main well-crystallized phases are detectable by XRD: for mixed materials, detection limit is about 1% of the sample. These data suggest a clear distinction of the composition of the clay-rich (Marcellus and Barnett) and carbonate-rich (Green River) shales between the different studied fields. XRD diffractograms of extraction residue samples from the unreacted shale and the reacted shale are similar for each shale. These diffractograms show, after chemical extraction, the occurrence of borates and sulfates, which are precipitated at the end of the extractions due to the addition of boric acid. The diffractograms are similar for the residues of the unreacted and the reacted shales.

We assume that uranium released from all extraction steps sums to the total uranium concentrations in the samples: 8.3 ppm for Marcellus, 2.2 ppm for Green River, 5.8 ppm for Barnett. Uranium extracted for each of the steps was quantified for unreacted and reacted shales (**Figure 14**). Three major conclusions arise immediately from the results: (i) fracture fluid removed a surprisingly large fraction of total uranium from the shales; (ii) the fraction of uranium extracted (out of total uranium in the sample) is highly variable for the different shale samples: 20% in Green River, 27% in Marcellus, and 57% in Barnett. (iii) In particular, the carbonate-rich shale released less uranium than the less reactive clay-rich shale matrices.

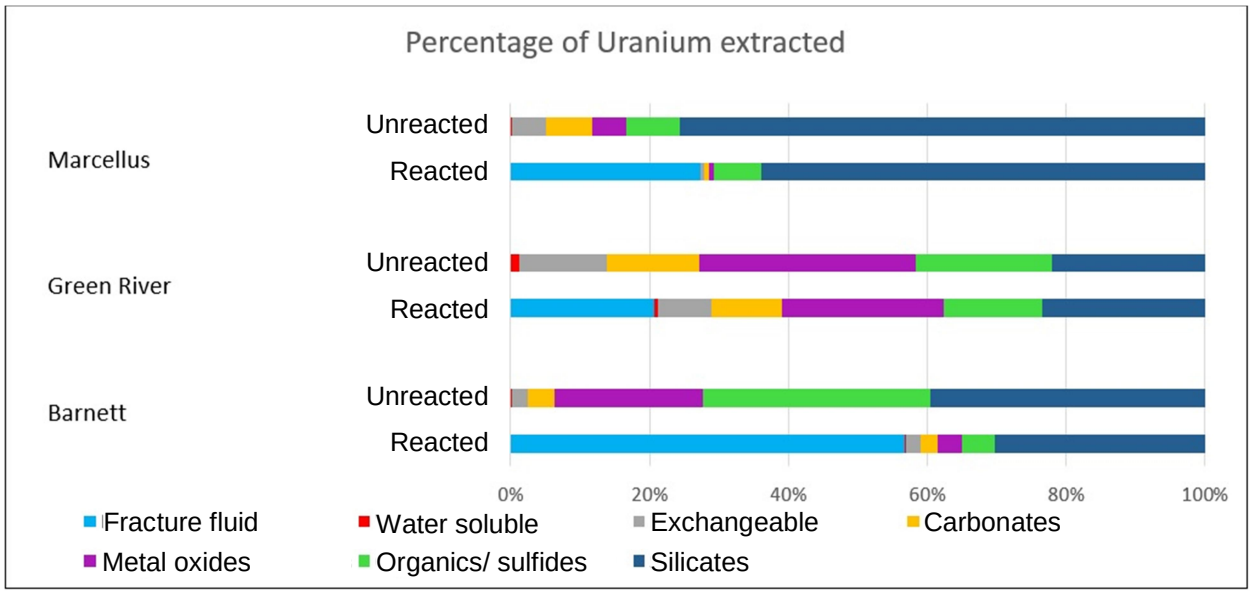

Figure 14 – Percentage of Uranium extracted during the different steps of the extractions for non-prereacted and fracture fluid-pre-reacted Marcellus, Green River and Barnett shales.

The main host minerals for uranium are silicates and then the organic matter and sulfides for the clay-rich shales. In contrast, for the carbonate-rich Green-River shale, uranium was primarily hosted in metal oxides and organic matter / sulfides. Although uranium is mainly hosted in silicates, especially for the clay-rich shales, this pool of uranium is relatively inaccessible to fracture fluid. In contrast, uranium was readily released from water soluble and from the exchangeable (clay) fractions. These highly reactive pools of uranium were present at variable concentrations in the different shale samples. In addition, the reactivity of the organic and the metal oxide fractions were highly reactive in the Barnett shale (and to a lesser extent in the

Marcellus), and much less reactive in the Green River shale. These observations help to explain the observed differences in total uranium extracted from the different shales.

One potential explanation for this behavior is incomplete removal of carbonate during the 3rd extraction step. Residual carbonate would react quickly with acid, helping to protect the other pools of uranium in the sample. In aggregate, these results suggest that siliceous shales, which are typically considered to be relatively unreactive as compared to carbonates, are likely to release more uranium (and other contaminants).

Manuscript plans. Results from quarters 1-5 have been incorporated into the manuscript from Tasks 4/6 that has been submitted to *Applied Geochemistry*. We are planning to write a second manuscript to detail the sequential extraction results during FY 2017.

Deliverables. The above-mentioned manuscripts are the primary deliverables from this task.

Task 6. Geochemical and transport modeling.

Geochemical modeling is being performed to support 1-D, 2-D, and 3-D representations of fractured shale in order to make predictions about the coupling between redox reactions, uranium transformations and transport of fracture fluids. A zero-dimensional model (including chemistry and reaction kinetics but no transport) was evaluated and calibrated using the experimental data from Task 4 to provide insight into the governing processes occurring upon exposure of shale to hydraulic fracturing fluid and provide a platform for future work coupling transport with geochemical processes. This effort is needed to provide thermodynamic and kinetic input parameters for reservoir simulations that include geochemical reactions.

Progress in quarters 5-7. To develop a framework for prediction and evaluation of our experimental studies, we used the multicomponent reactive transport code Crunch Flow (Steefel *et al.*, 2014) to create a set of mixed kinetic-equilibrium reaction path calculations that include shale mineralogy, aqueous species and secondary mineral phases likely to form when shales interact with oxidized fracture fluids. Thermodynamic data are from the EQ3/EQ6 database and the kinetic data (including rate constants, activation energies and any dependence on aqueous species) were compiled and evaluated using the compilation of Palandri and Kharaka (2004).

Model constructs were used in the past year to generate insight as to the governing chemical processes occurring in our experiments. This was accomplished via 1) simulation of experimental conditions (Task 4 experiments) using a zero-dimensional kinetic model, 2) sensitivity analysis of model results to variations in solid and gas chemistry, and 3) speciation of solutes released into experimental fluids to elucidate mineral dissolution-precipitation reactions occurring in the experiments. Completion of these activities positioned us to write and submit a manuscript,for publication, which includes the complementary experimental results in Task 4.

Progress in quarter 8. The focus of the 8th quarter was in preparing the manuscript. The initial draft of the manuscript was completed and revised. This manuscript has been submitted to *Applied Geochemistry*. A new postdoctoral scholar was hired in September to begin planning and conducting the next phase of our modeling program, which will involve reacting whole cores with fracture fluid, characterizing formation damage and permeability, and modeling the impact of these changes on transport across shale matrix-fracture interfaces. As part of her start-up activities, the new postdoc evaluated both modeling and experimental approaches for

investigating impact of secondary porosity on permeability. This activity is continuing in the renewed project.

Table 5. Task 6 objectives for quarters 5-8. Objectives completed in quarter 8 are indicated with bolded text.

Goal	Status
Develop model using incoming experimental data	Complete
Use model to inform experimental interpretations	Complete
Sensitivity analysis	Complete
Model refinement	Complete
Evaluate model/experimental approaches for investigating impact of secondary porosity on permeability	Complete
Draft manuscript	Complete
Submit manuscript	**Complete**

Results.

Batch modeling of experimental conditions

Published kinetic dissolution-precipitation rate laws for mineral phases present in the shales and secondary precipitates were input into CrunchFlow (Steefel *et al*., 2014) to simulate time-dependent trends in cation and anion concentrations. In order to reproduce the observed absolute concentrations of solutes, the reactive surface area of dissolving minerals was adjusted in the models. This is a typical approach employed in reactive transport modeling applications.

Calcium concentrations and pH predicted by modeling agreed fairly well with observation, confirming that calcium and alkalinity were primarily generated via calcite dissolution, and that calcite dissolution was not strongly impacted by the additives present in the fracture fluid. Similarly, the presence of O_2 was found not to strongly impact calcite dissolution for the Barnett and EF shales **(Figure 18)** (this was not examined experimentally for GR). Significant differences between O_2-rich, O_2-limited, and O_2-free Marcellus-bearing experiments were evident. In particular, different amounts of Ca^{2+} were released (**Figure 18**). Modeling confirmed that this was most likely due to different initial abundance of calcite in Marcellus samples used between experiments, rather than a true consequence of O_2 availability. Together, these results illustrated that calcite dissolution occurs rapidly (on a time scale of hours) upon exposure of carbonate-bearing shales to acidic hydraulic fracturing fluid, and its dissolution strongly controls the evolution of fluid composition, most importantly with respect to pH. The evolution of fluid pH is therefore highly sensitive to minor variations in carbonate mineral content, and may vary spatially at the pore-scale as dictated by mineralogical heterogeneity of the shale matrix.

There was significant mismatch between model-predicted and observed Fe concentrations for the Barnett and Marcellus shales (Fe concentrations were below our instrument detection limits

for the EF and GR, hindering comparison with model output). Iron and sulfate are sourced largely from the dissolution of pyrite. Therefore, concentrations of sulfate (SO_4^{2-}) provide insight into the behavior of Fe. Sulfate concentrations were reproduced well for the Barnett shale, indicating that the model was capturing pyrite dissolution behavior. However, Fe concentrations were consistently higher than predicted by the model for Barnett shale. For Marcellus shale, Fe concentrations were again underestimated by the model for all scenarios of O_2 availability, and sulfate overestimated except in the case of the O_2-free reactors (**Figure 19**). These results imply that even when pyrite dissolution rates are well represented in the model, the rate of precipitation of secondary Fe(III)-bearing minerals, and/or the rate of aqueous Fe(II) oxidation is consistently faster in the models than the experiments. In addition, there may be complexes forming between aqueous Fe and organic components of the shales and fracture fluids that cause a greater proportion of Fe to remain in solution than expected. At present, we are unable to separate these effects with modeling alone, highlighting a key knowledge gap to be addressed with future research.

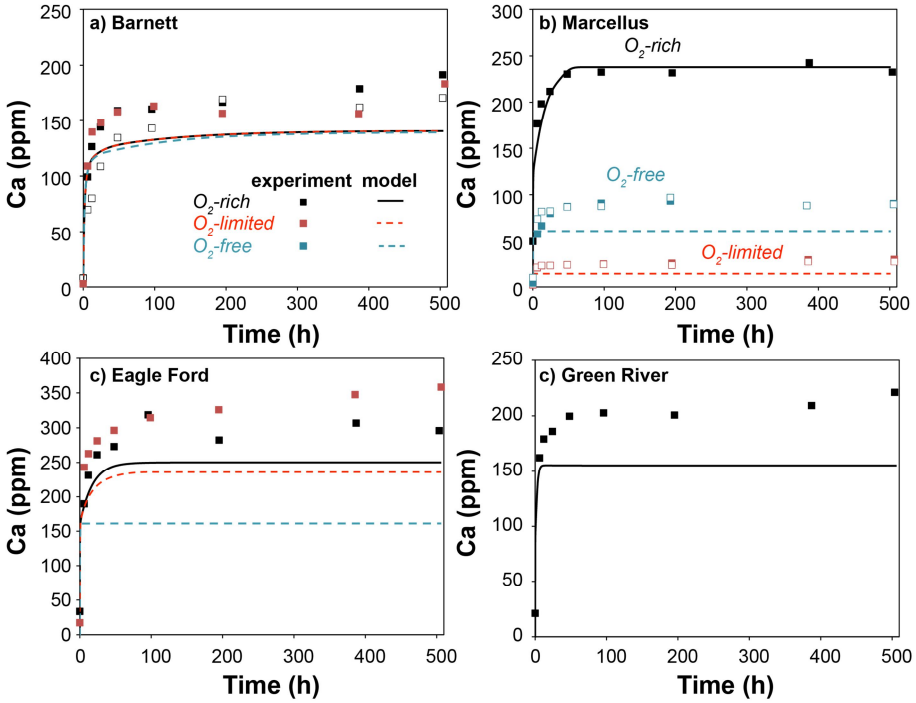

Figure 18. Comparison of modeled versus experimental aqueous calcium (Ca) concentrations for short-term O_2-rich (black data), O_2-limited (red data), and O_2-free conditions (blue data). O_2-free conditions were only conducted experimentally for the Marcellus shale, but model predictions for these conditions are shown for the Marcellus, Barnett, and Eagle Ford shales. Experimental data are represented by squares, whereas model output is shown by lines. Duplicate experiments are represented by open squares. Analytical uncertainty is smaller than symbol size.

Sensitivity analysis

Our experimental and modeling results have revealed that the initial abundance of carbonate in the shale is a major control on the subsequent evolution of the reservoir, not only in terms of porosity generation, but also on contaminant release and secondary phase precipitation. This is attributed in large part to the buffering capacity of carbonate minerals; dissolution of carbonate minerals helps to recover fracture fluid pH to circum-neutral values. However, oxidative

dissolution of pyrite, and subsequent Fe(III)-(oxy)hydroxide precipitation generates acidity, and can counter the buffering effect of carbonate dissolution. The pH evolution of a shale reservoir is therefore likely to depend strongly on the ratio of available carbonate to pyrite (and other redox-sensitive minerals). The "availability" of these phases depends on their abundance, reactive surface area, distribution, and accessibility to the reactive fluid.

To assess the relative importance of carbonate and pyrite abundance on reservoir evolution, a sensitivity analysis was conducted in which the reactive surface areas and abundance of these phases was adjusted and the subsequent change in dissolved Ca^{2+} concentrations (a proxy for solutes in general) were tracked. The outcomes of this analysis are compared in **Figure 20** for a carbonate-rich (Eagle Ford) versus carbonate-poor (Barnett) shale.

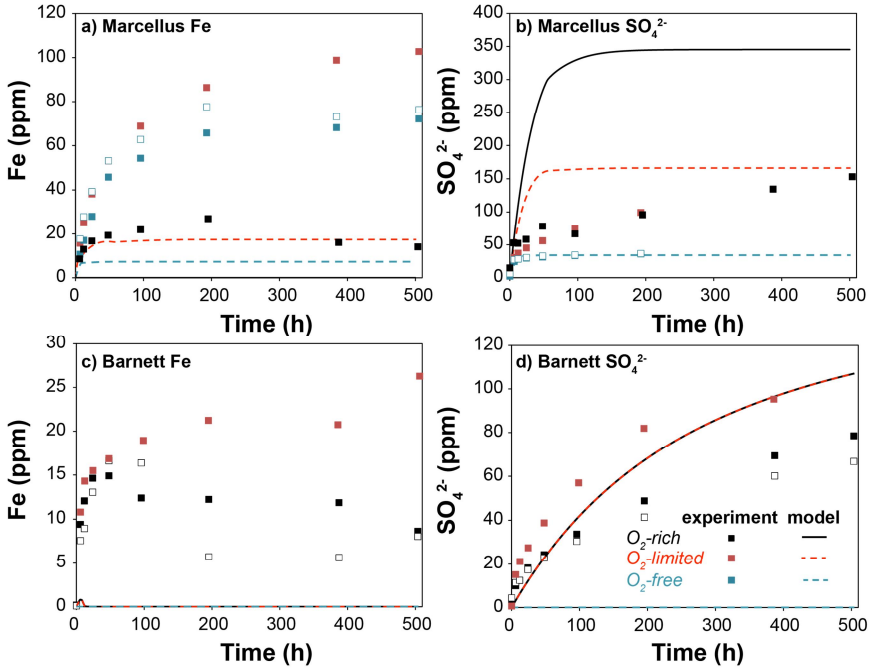

Figure 19. Comparison of modeled versus experimental aqueous iron (Fe) concentrations for the Marcellus (a) and Barnett (c) shales for the short-term O_2-rich (black data), O_2-limited (red data), and O_2-free conditions (blue data). O_2-free conditions were only conducted experimentally for the Marcellus shale, but model predictions for these conditions are shown for the Marcellus and Barnett shales. Experimental data are represented by squares, whereas model output is shown by lines. Duplicate experiments are represented by open squares. Analytical uncertainty is smaller than symbols.

The sensitivity analysis revealed that the extent of shale alteration is highly dependent on the mineralogical composition and the accessibility of the highly reactive phases (pyrite and carbonates) to the fracturing fluid. In addition, the level of contaminant release will be highly sensitive to the relative abundance of acid generating reactants (*e.g.*, pyrite) and buffering agents (*e.g.*, carbonate) and their degree of exposure to the fracturing fluid. Namely, modeling revealed that solute release from carbonate-rich shales is not strongly affected by accessible carbonate volume, yet solute release from carbonate-poor shales is strongly affected by minor changes in accessible carbonate volume, On the other hand, solute release from carbonate-poor shales is less

sensitive to changes in accessible pyrite than carbonate-rich shales **(Figure 20).** In both cases, this is related to the much higher pH-buffering capacity of carbonate rich shales. The implication is that the extent of porosity alteration of carbonate-poor shales will depend much less strongly on relative pyrite abundance and the availability of oxidants (*e.g.*, O_2) than will carbonate-rich shales. From an operations perspective, this result indicates that during acidization of shales, a common practice prior to injection of fracture fluid, the solute release and degree of porosity alteration will depend strongly on the mineral composition and distribution of minerals in the shale. Heterogeneity in carbonate content, as observed in the carbonate-poor Marcellus shale, may lead to significantly different chemical responses of the reservoir to acidization between wells within the same formation owing to only minor differences in carbonate mineral content.

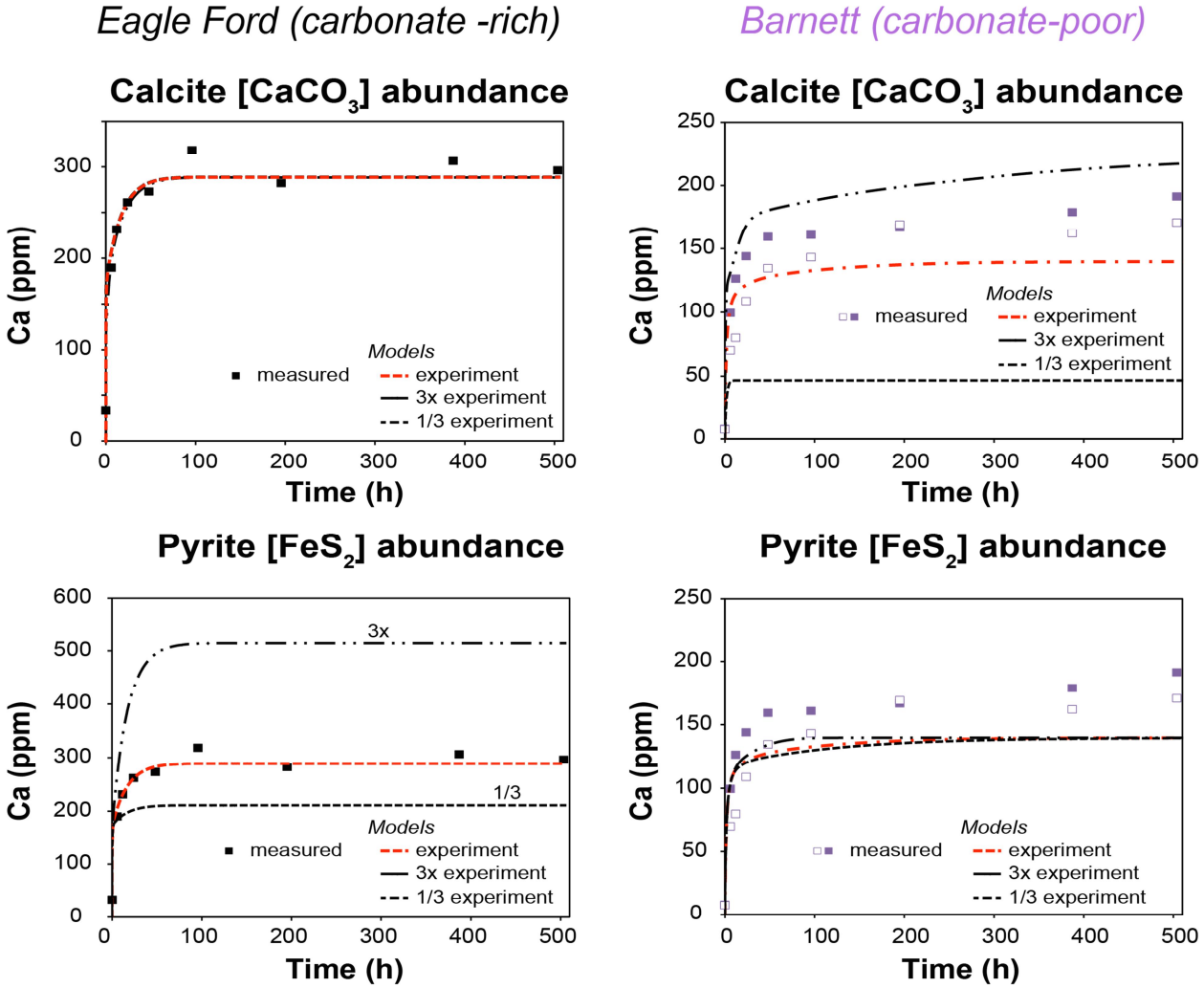

Figure 20. Sensitivity analysis illustrating the impacts of calcite [$CaCO_3$] and pyrite [FeS_2] abundance on shale reservoir chemistry for a carbonate-rich (Eagle Ford) versus carbonate-poor (Barnett) shale. Results are shown in terms of aqueous calcium (Ca) concentrations versus time, with model output shown by dashed lines and experimental data shown as points. In each case, either calcite or pyrite abundance was adjusted by a factor of three above or below the measured experimental abundance (red dashed line). In the case of the carbonate-rich Eagle Ford shale, a 3-fold increase or decrease in the total amount of carbonate present has no effect on the dissolved Ca^{2+}. Carbonate is so abundant that it controls Ca^{2+} at a

solubility limit, even for the lowest concentration used in the simulations. In contrast, in the case of carbonate-rich Barnett shale, carbonate is quickly consumed, and Ca^{2+} is released to aqueous solution.

Speciation calculations

Porosity-occluding reactions. The oxidative dissolution of pyrite is commonly accompanied by precipitation of secondary Fe(III)-bearing (hydr)oxide phases (Blowes *et al*., 1998; Nordstrom, 1982), which provides the potential to clog pore spaces and inhibit hydrocarbon and contaminant transport. Contaminant release may also be attenuated via co-precipitation with or sorption on hydroxide mineral surfaces. Spectroscopic and aqueous chemical data confirmed the presence of Fe(III)-bearing secondary minerals in shales after reaction with hydraulic fracturing fluid for all four shale types. Speciation calculations revealed that amorphous $Fe(OH)_3$ became supersaturated in Marcellus and Barnett reactors within 24 h **(Figure 21)**. Though the lack of aqueous Fe data for the Eagle Ford and Green River experiments precludes direct calculation of the saturation indices of Fe-bearing minerals, the pH of these fluids means that Fe(III)-hydroxides could be stable even with Fe concentrations below our analytical detection limits. The removal of iron from solution in the Marcellus, Barnett, and Eagle Ford experiments is thus inferred to reflect the precipitation of secondary Fe(III)-(oxy)hydroxide phase(s), which were manifested as rust-colored solids observed in the experiments. The crystalline phases goethite and hematite were highly supersaturated in the Marcellus and Barnett experiments, as indicated by saturation indices >> 1.0 **(Figure 21).** In contrast, the saturation state of amorphous $Fe(OH)_3$ declined towards equilibrium in the short-term experiments (<500 h), indicating that the precipitates were likely amorphous or poorly crystalline Fe(III)-(oxy)hydroxide, or that Fe(II) oxidation to Fe(III) was relatively slow (*i.e.* not at equilibrium) causing over estimation of saturation state. Similarly, aqueous complexes formed between organic in the fracture fluid and shale with Fe may result in overestimation of the saturation state of Fe-bearing minerals, as these cannot presently be accounted for due to a lack of thermodynamic data. The lack of measurable aqueous Fe throughout the Eagle Ford experiments and the decline in Fe concentration after 95 h in the Marcellus experiment nevertheless implies that precipitation of an Fe(III)-bearing phase began at least within 95 h. This suggests Fe(oxy)hydroxides could form within hours of hydraulic fracturing, and could have abrupt consequences on the transport and recovery of hydrocarbons and the composition of flowback and produced waters.

Speciation calculations revealed that no sulfate-bearing minerals were saturated in the bulk solutions for all shales, yet precipitates composed of Ca, S, and O were identified with scanning electron microscopy and energy dispersive spectroscopy in Barnett samples from the long-term experiments. As such, it is not certain whether these precipitates formed *in situ* during the experiments, or were an artifact formed when the samples were dried following the experiment.

Porosity-generating reactions. Based on aqueous chemical data and XRF and XRD analyses of reacted shales, it was concluded that calcite dissolution was the primary source of dissolved Ca for all experiments. Yet, the occurrence of plateaus in Ca concentration, and the magnitude of Ca concentration at these plateaus are attributed to different factors between the carbonate-rich and carbonate-poor shales.

Speciation calculations revealed that coincident Ca concentration and circumneutral pH plateaus for the carbonate-rich shales (Eagle Ford and Green River) were associated with achievement of equilibrium with respect to calcite **(Figure 22)**; the fluid reached saturation with respect to calcite within 48 h and remained approximately at equilibrium throughout the

remainder of the short-term experiments. Similarly, fluids remained approximately at equilibrium with respect to calcite throughout the intermediate- and long-term Eagle Ford and Green River experiments. In contrast, the solutions remained undersaturated with respect to calcite for experiments of all durations containing the carbonate-poor Barnett and Marcellus shales **(Figure 23)**. Mass balance calculations based on XRF analysis of the initial materials and final aqueous Ca concentrations revealed that these carbonate-poor shales were almost completely stripped of Ca within three weeks, whereas the carbonate-rich Eagle Ford and Green River shales maintained greater than 70% of their initial Ca. The plateaus in Ca concentration and pH are attributed to the exhaustion of the accessible calcite for the carbonate-poor shales, and to the achievement of equilibrium with respect to calcite for the carbonate-rich shales. The magnitude of the Ca concentration at these plateaus is therefore dictated by the mass of fluid-accessible calcite for the carbonate-poor shales, and the extent of dissolution required toachieve equilibrium for the carbonate-rich shales.

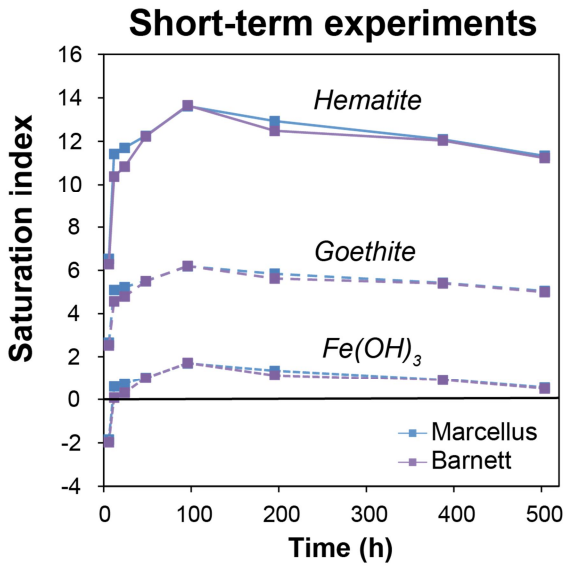

Figure 21. Saturation indices of secondary Fe(III)-bearing phases versus time in the short-term Marcellus (a) and Barnett (b) experiments. The solid black line indicates chemical equilibrium with respect to a given solid phase (*i.e.* saturation index = 0).

Calcite dissolution generates alkalinity, yet the oxidative dissolution of pyrite generates acidity. Both these reactions were documented to occur on a similar timescale (<100 hours) in all experiments with pyrite-bearing shales. The pH of the fluid at “steady-state” reflects the balance between the extent of pyrite dissolution and the abundance of calcite available to buffer the fluid pH. In the case of the carbonate-poor shales, fluids remained acidic as there was insufficient calcite available to counterbalance the combined acidity of the initial fracturing fluid and that generated from pyrite oxidation. Conversely, the carbonate-rich Eagle Ford and Green River shales had sufficient alkalinity-generating capacity to neutralize all acidity. The extent of calcite dissolution that occurs in a shale formation will therefore depend on the initial pH and volume of the injected fluid, as well as the abundance of pyrite and amount of dissolved oxygen in the injected fluids.

Notably, the other carbonate minerals, dolomite and magnesite remained undersaturated in all experiments, with the exception of the Green River experiments, for which dolomite was slightly supersaturated. The saturation state of siderite [$FeCO_3$] could not be calculated for the Eagle Ford and Green River experiments due to the lack of aqueous Fe data, but it remained undersaturated in the Barnett and Marcellus experiments. This implies, that although dissolution of these other carbonate minerals likely occurred, calcite exerted the strongest control on overall fluid pH and Ca concentrations.

Manuscript plans. A manuscript has been submitted to *Applied Geochemistry* including the speciation modeling results and data from Tasks 4 and 5. A second manuscript is being prepared for submission to *Environmental Science and Technology* that will include additional modeling results. It is expected that this will be submitted in early 2017.

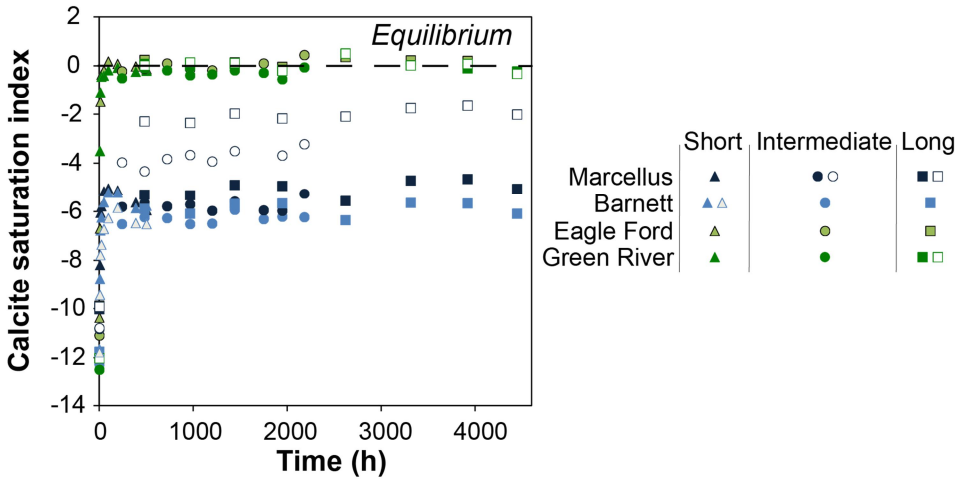

Figure 22. Saturation index of calcite [$CaCO_3$] in all experiments. Data from the short-, intermediate-, and long-term experiments are represented by triangles, circles, and squares, respectively. Duplicate reactors are distinguished by filled versus unfilled symbols of the same type. The black dashed line indicates chemical equilibrium with respect to calcite (*i.e.* saturation index = 0)

Deliverables. The geochemical modeling results are included in a manuscript generated with results from Task 4 (bulk shale-fracture fluid interactions). This work, along with that from Task 4, was presented in oral format at the Goldschmidt International Geochemistry Conference in June 2016 in Yokohama, Japan. It will also be presented at the 2016 American Geophysical Union Annual Conference in San Francisco in December in oral format.

References:

Palandri, J.L., Kharaka, Y.K., 2004. A compilation of rate parameters of water-mineral interaction kinetics for application to geochemical modeling. Menlo Park, California.

Steefel, C.I., Druhan, J.L., Maher, K., 2014. Modeling Coupled Chemical and Isotopic Equilibration Rates. Procedia Earth Planet. Sci. 10, 208–217.

Nordstrom, D. K., 1982. Aqueous pyrite oxidation and the consequent formation of secondary iron minerals. Acid sulfate weathering, 37-56.

Blowes, D.W., Jambor, J.L., Hanton-fong, C.J., Lortie, L., Gould, W.D., 1998. Geochemical , mineralogical and microbiological characterization of a sulpide-bearing carbonate-rich gold-mine tailings impoundment, Joutel, Quebec. Appl. Geochemistry 13, 687–705.

4. RISK ANALYSIS

Task 1. Project management plan

Summary description: The Recipient shall work together with the NETL project manager to maintain and update the project management plan (PMP) originally submitted at FWP approval (and formatted in accordance with the guidance provided by NETL).

Project management risks: Post-doctoral departures mid-term, increased risk from short-duration of project, and user facility access risks.

Project resource limitation risks: publication risk

Mitigation:

(i) *Publication risk.* Time is was allocated to write manuscripts because experiments will not be complete until the end of the 18-month period. For this reason, we are requesting a no-cost extension of the project.

Publication risk is a concern because it undermines recruiting and retention efforts and decreases the scientific stature of the home institution and funding agency. Additional risks to publications include (a) departures of post-doctoral fellows prior to completion of manuscripts, (b) failure to complete experiments on the proposed timeline, and (c) insufficient quality of experimental results for publication.

Mitigation: Requeset no-cost extension of project to end of FY2016. In addition, to address (a), post-doctoral scholars are presently outlining the intended manuscripts and experiments and data collection are being specifically targeted to fill gaps in the current data set to allow for manuscripts to be written. In addition, writing of manuscripts is scheduled to begin prior to the end of the project timeline (and post-doctoral departures) in order to maximize the amount of writing completed while the project is still active and the research group is intact. To address (b), the experimental plan has been refined such that only the key experiments required to produce the desired manuscripts will be conducted (*e.g.*, pure mineral experiments were excluded from Task 2). Moreover, the majority of the planned experiments have either been completed, or are already underway. Finally, to address (c), analysis of the experimental results has been ongoing throughout the project to ensure that the data produced is of value, and the experimental designs are sufficient to produce the necessary quality of data. For example, the experimental design for Task 4 experiments has been altered in order to better constrain the O_2 available for reaction. The coincidence of experiments and analysis permits rapid adjustment of experimental protocols to ensure the data produced are relevant and of good quality.

(ii) *Post-doctoral departures mid-term*. Post-doctoral researchers may depart the project mid-term, creating new recruiting needs and pushing back critical path.

Mitigation: (a) maintain communication with post-doctoral researchers to discover departures as soon as possible, (b) initiate recruiting efforts as soon as possible to fill vacancies, (c) redirect graduate students and remaining staff to maintain critical-path progress during vacancies.

(iii) *Increased exposure to risks in (i) due to short project duration.* The short project duration decreases the time available to respond to the above risk. *Mitigation*: (a) Emphasize initial planning, (b) Emphasize project management for on-time progress, and (c) actively prioritize experimental plans to target most promising research directions.

(iv) User facility access risk. Obtaining access to user facilities such as ALS (advanced light source) requires long lead-times, typically 6 months. *Mitigation*: (i) leverage existing facility access proposals on other projects to initiate measurements at user facilities, (ii) use alternative characterization techniques if necessary.

Task 2. Fe(II) and bitumen reactions with fracture-fluid

Summary description: Research for this task has been refocused on assessing rates of aqueous Fe(II) oxidation in the presence of hydraulic fracture fluid additives and the bitumen inherent to the shales. Preliminary results demonstrated that the combination of bitumen and hydraulic fracture solution can accelerate Fe(II) oxidation compared to solutions lacking these organics. As the kinetics of aqueous Fe oxidation is one of the main unknowns in the reaction network, which hinders modeling and prediction of reaction progress, these experiments are viewed as a key step towards better understanding the controls on reactions in these environments. Mineral reaction kinetics are comparatively better understood.

Technical risks: Experimentation is complete: No risks to report.

Mitigation: Not applicable.

Task 3: Kerogen-fracture fluid interactions

Summary description: High purity kerogen has been isolated from Marcellus and Green River shales and reacted with fracture fluid for varying lengths of time following the procedure described in Task 3.

Technical risks: Experimentation is complete: No risks to report.

Mitigation: Not applicable.

Task 4: Whole shale-fracture fluid interactions

Summary description: This module investigated the impact of fracture fluids on whole shales with emphasis on identifying the key reactions that could driving porosity/permeability changes and metal release.

Technical risks: Experimentation is complete: No risks to report.

Mitigation: Not applicable.

Task 5: Uranium-fracture fluid interactions

Summary description: A subset of the unreacted and reacted shale samples produced in task 4 were analyzed by sequential extraction to identify the specific mineral hosts in the shale and evaluate the risks of release based on observed reaction rates of these host minerals.

Technical risks: Milestones are complete. No risks to report.

Mitigation: Not applicable.

Task 6: Geochemical modeling to describe interactions between fracture fluid and shale

Summary description: A geochemical model has been developed to describe interactions between the key components of fracture fluid and shale. Forward models of experiments assisted researchers in evaluating the optimal conditions for the experiments (initially) as well as the kinetics and equilibrium points. Ultimately, the calibrated model can be used to evaluate 2-D and 3-D representations of fractured shale in order to make predictions about the coupling between redox reactions, uranium transformations and transport of fracture fluids. The model will be evaluated and calibrated using the experimental data providing a platform for future work linking transport and geochemical processes.

Technical risks: Modeling complete: No risks to report.

Mitigation: Not applicable.

5. MILESTONE STATUS

Activity and milestones	Verification method†	Planned Milestone Date	Actual completion or status*
Task 1. Project management			
1.1 Development of PMP	D	10-1-14	10-1-14
1.2 Quarterly research performance reports	D	8-30-15‡	8-30-15
1.3 Annual research performance report	D	10-31-15	11-30-15
1.4 Final technical report	D	11-30-16	11-30-16
Task 2.			
2.1 Isolation of bitumen	C	4-30-15	3-31-15
2.2 Develop model fracture fluid recipe	D	1-15-15	1-15-15
2.3 Reaction of Fe(II) solution with hydraulic fracturing solution	C	10-15-15	10-20-15
2.4 Reaction of Fe(II) with hydraulic fracturing solution and/or bitumen [Set I]	R	3-31-16	11-15-15
2.5 Reaction of Fe(II) with hydraulic fracturing solution and/or bitumen at varied DO [Set II]	R	4-30-16	4-20-16
2.6 Characterization of alterations to bitumen and hydraulic fracturing solution during Fe(II) oxidation	FTIR, STXM	7-31-16	4-20-16
2.7 Characterization of Fe reaction products	XRD, FTIR	7-31-16	4-11-16
2.8 Initial draft of Fe(II)-bitumen manuscript		8-31-16	8-18-16
2.9 Submission of Fe(II)-bitumen manuscript		10-30-16	11-30-16
Task 3.			
3.1 Isolation of kerogen from Green River (GR) shale	K	4-30-15	3-31-15
3.2 Completion of short-term fluid- GR kerogen reactions	C	6-30-15	6-16-15
3.3 Completion of intermediate-term GR kerogen reactions	C	8-31-15	9-3-15
3.4 Isolation of kerogen from Marcellus shale	K	9-30-15	11-30-15
3.5 Completion of long-term GR kerogen fluid-kerogen reactions	C	11-30-15	11-15-15
3.6 Completion of short-term fluid- Marcellus kerogen reactions	SS, G	12-15-15	12-18-15
3.7 Characterization of samples, solute data	So, XPS, SEM, EDS	3-31-16	10-30-16
Tasks 4 and 5.			
4.1 Initial characterization of shales	XRD, XRF	4-30-15	3-31-15
4.2 Initial short (2 week) reaction with HCl-only	S	4-30-15	3-31-15
4.3 Analysis of reaction products from initial reaction	So	4-30-15	3-31-15
4.4 Completion of short-term fluid-shale reactions	So, XPS, SEM, EDS	6-30-15	6-16-15
4.5 Completion of short-term fluid-shale reactions with closed headspace [Set II]	S	10-31-15	12-17-15
4.6 Completion of short-term fluid-shale reactions with closed headspace (Marcellus repeat) [Set III]	S	5-31-16	5-22-16
4.7 Completion of intermediate-term reactions	SS, G	8-31-15	9-3-15
4.8 Completion of long-term fluid-shale reactions	SS, G	11-30-15	12-5-15

4.9 Characterization of shale samples, solute data	So, XPS, SEM, EDS	7-31-16	3-21-16
4.10 Sequential Chemical Extractions (Task 5 only)	So	7-31-16	7-11-16
4.11 Characterization of uranium samples (Task 5 only)	R	7-31-16	7-18-16
4.12 Complete manuscript draft	D	6-30-16	6-30-16
4.13 Submit manuscript	D	10-31-16	11-30-16
Task 6.			
6.1 Complete initial modeling for experiment design	P	1-31-15	1-31-15
6.2 Completion of numerical experiments	P	12-31-15	12-31-15
6.3 Evaluate models against experimental data	P	3-31-16	4-30-16
6.4 Conduct sensitivity analyses	P	3-31-16	4-30-16
6.5 Model refinement	P	7-31-16	10-30-16
6.6 Complete initial model development for secondary porosity simulation task	D	10-31-16	10-30-16

† Verification methods: D**,** Documentation; S, Samples harvested; C, complete; R, characterization results in-hand; K, extracted kerogen available; P, simulation results plotted; XRD, X-ray diffraction data collected; XRF, X-ray fluorescence data collected; SEM, scanning-electron microscopy data collected; SS, solute samples collected; So, solute data collected; G, gas samples collected; XPS, X-ray photoelectron spectroscopy data collected; EDS, energy dispersive spectroscopy data collected; M, manuscript in-hand.

* Status as of Oct 30, 2015.

‡ Future quarterly report dates: in 2015: Oct 30; in 2016: Jan 30

6. SCHEDULE STATUS

All milestones have been completed. As noted in a communication dated Feb 26, 2016, we extended the project duration to September 30, 2016. At that time, we added an additional task to the program schedule and management plan, namely Task 6.6, "Complete initial model development for secondary pore simulation task". This activity was subsequently retitled as, "Complete initial model development for secondary porosity simulation task" in response to discussions with program management in June 2016.

Project timeline from the Project Management Plan. "M" denotes milestones.

Task	Title	Month of project																								
					2015													2016									
	Quarter:	1			2			**3**			4			5			6			7			8			
	Month:	1	2	3	4	5	6	7	8	9	10	11	12	13	14	15	16	17	18	19	20	21	22	23	24	
		Oct	Nov	Dec	Jan	Feb	Mar	Apr	May	June	July	Aug	Sept	Oct	Nov	Dec	Jan	Feb	Mar	Apr	May	June	July	Aug	Sept	
1	Project management plan																									
	Development and revision	M																								
	Quarterly progress reports				M			M			M			M			M			M			M			
	Annual progress reports													M												M
	Final technical report																									M
	Ongoing project management																									
2	Mineral-fracking fluid																									
2.1	Initial characterization (XRD)				M																					
2.2	Develop model fracking fluid																									
2.3	Reaction of Fe(II) solution with hydraulic fracturing solution													M												
2.4	Reaction of Fe(II) w/bitumen [Set I]																		M							
2.5	Reaction of Fe(II) w/bitumen [Set II]																			M						
2.6	Characterization of alterations to bitumen																						M			
2.7	Characterize Fe products																						M			
2.8	Draft manuscript																						M			
2.9	Manuscript submission																									M
3	Kerogen-fracking fluid																									
3.1	Isolation of Green River kerogen (GRK)							M																		
3.2	Short-term GRK experiment															M										
3.3	Intermediate-term GRK experiment											M														
3.4	Isolation of Marcellus kerogen (MK)															M										
3.5	Long-term GRK experiment														M											
3.6	Short-term MK experiment																	M								
3.7	Characterization																									M
4	Whole shale-fracking fluid																									
4.1	Initial characterization							M																		
4.2	Initial 2-wk HCl-only reaction							M																		
4.3	Analysis of reaction products							M																		
4.4	Short-term experiment [I]										M															
4.5	Short-term experiment [II]													M												
4.6	Short-term experiment [III]																				M					
4.7	Intermediate-term experiment											M														
4.8	Long-term experiment														M											
4.9	Characterization																						M			
4.10	(Task 5 only)																									
4.11	(Task 5 only)																									
4.12	Draft manuscript																						M			
4.13	Manuscript submission																									M
5	Uranium-fracking fluid																									
5.1	Initial characterization							M																		
5.2	Initial 2-wk HCl-only reaction							M																		
5.3	Analysis of reaction products							M																		
5.4	Short-term experiment										M															
5.5	Short-term experiment [II]															M										
5.6	Short-term experiment [III]															M										
5.7	Intermediate-term experiment											M														
5.8	Long-term experiment														M											
5.9	Characterization																						M			
5.10	Sequential extractions																						M			
5.11	U Characterization																						M			
5.12	Draft manuscript																						M			
5.13	Manuscript submission																									M
6	Modeling																									
6.1	Initial numerical experiments for experiment design				M																					
6.2	Numerical experiments																M									
6.3	Evaluate models against data																				M					
6.4	Sensitivity analysis																				M					
6.5	Model refinement																						M			
6.6	Complete initial model: secondary porosity simulation																									M

7. COST STATUS

Cost Plan/Status

Baseline Reporting Quarter		Year 1	Start: 9/1/14	End: 9/30/14		Year 2		Start: 10/1/15	End: 9/30/16		Year 3		Start: 10/1/15	End: 9/30/16	
		Q1	Q2	Q3	Q4	Q5	Q6	Q7	Q8	Q9	Q10	Q11	Q12		
Baseline Cost Plan															
Federal Share	Task 1					$ 2,709	$ 3,195	$ 4,744	$ 14,453	$ 8,846	$ 8,846	$ 8,846	$ 8,846		
	Task 2					$ 5,743	$ 6,773	$ 10,058	$ 30,641	$ 14,941	$ 12,105	$ 12,105	$ 12,105		
	Task 3					$ 4,931	$ 5,815	$ 8,635	$ 26,305	$ 10,292	$ 10,292	$ 10,292	$ 10,292		
	Task 4					$ 5,743	$ 6,773	$ 10,058	$ 30,641	$ 12,165	$ 12,165	$ 12,165	$ 12,165		
	Task 5					$ 5,743	$ 6,773	$ 10,058	$ 30,641	$ 12,165	$ 12,165	$ 12,165	$ 12,165		
	Task 6					$ 2,221	$ 2,620	$ 3,890	$ 11,852	$ 5,964	$ 5,964	$ 5,964	$ 5,964		
Non-Federal Share															
Total Planned Costs (Federal and Non-Federal)															
Cumulative Baseline Cost		$ -	$ -	$ -	$ -	$ 27,091	$ 59,040	$106,484	$251,017	$315,390	$376,927	$438,464	$540,000		
Actual Incurred Costs															
Federal Share	Task 1					$ 2,709	$ 3,195	$ 4,744	$ 14,453	$ 5,813	$ 5,119	$ 5,256	$ 6,920		
	Task 2					$ 5,743	$ 6,773	$ 10,058	$ 30,641	$ 12,323	$ 10,852	$ 11,143	$ 14,671		
	Task 3					$ 4,931	$ 5,815	$ 8,635	$ 26,305	$ 10,579	$ 9,316	$ 9,566	$ 12,595		
	Task 4					$ 5,743	$ 6,773	$ 10,058	$ 30,641	$ 12,323	$ 10,852	$ 11,143	$ 14,671		
	Task 5					$ 5,743	$ 6,773	$ 10,058	$ 30,641	$ 12,323	$ 10,852	$ 11,143	$ 14,671		
	Task 6					$ 2,221	$ 2,620	$ 3,890	$ 11,852	$ 4,766	$ 4,197	$ 4,310	$ 5,675		
Non-Federal Share															
Total Incurred Costs - Quarterly (Federal and Non-Federal)															
Cumulative Incurred Cost		$ -	$ -	$ -	$ -	$ 27,091	$ 31,949	$ 47,444	$144,533	$ 58,127	$ 51,187	$ 52,562	$ 69,204		
Variance															
Federal Share	Task 1	$ -	$ -	$ -	$ -	$ -	$ -	$ -	$ -	$ 3,033	$ 3,727	$ 3,589	$ 1,925		
	Task 2	$ -	$ -	$ -	$ -	$ -	$ -	$ -	$ -	$ 2,618	$ 1,253	$ 962	$ (2,566)		
	Task 3	$ -	$ -	$ -	$ -	$ -	$ -	$ -	$ -	$ (287)	$ 976	$ 725	$ (2,303)		
	Task 4	$ -	$ -	$ -	$ -	$ -	$ -	$ -	$ -	$ (158)	$ 1,313	$ 1,022	$ (2,506)		
	Task 5	$ -	$ -	$ -	$ -	$ -	$ -	$ -	$ -	$ (158)	$ 1,313	$ 1,022	$ (2,506)		
	Task 6	$ -	$ -	$ -	$ -	$ -	$ -	$ -	$ -	$ 1,198	$ 1,767	$ 1,654	$ 290		
Non-Federal Share		$ -	$ -	$ -	$ -	$ -	$ -	$ -	$ -	$ -	$ -	$ -	$ -		
Total Variance - Quarterly (Federal and Non-Federal)		$ -	$ -	$ -	$ -	$ -	$ -	$ -	$ -	$ -	$ -	$ -	$ -		
Cumulative Variance		$ -	$ -	$ -	$ -	$ -	$ -	$ -	$ -	$ 6,245	$ 16,595	$ 25,569	$ 17,902		

Collaborative Leveraging. The project effort was supported by 2 collaborating postdoctoral fellows (Andrew Kiss, and Arjun Kohli, SLAC), funded by a non-NETL program, and by 3 graduate students in the groups of Gordon Brown and Kate Maher (Stanford): Megan Dustin, Claresta Joe-Wong, and Dana Thomas. We also benefitted immensely from unfunded collaborations with Dr. Mark Zoback (Stanford).

8. CONCLUSIONS

Fluid-shale reactions drive changes in the mechanical stability, mineralogy, and porosity of shale and have the potential to release contaminants to flowback. Fluid-shale reactions are thus profoundly important to extraction technologies for producing natural gas and oil from unconventional reservoirs. Prior to this project, no studies had systematically investigated the geochemical reactions in shale driven by fracture fluid.

This NETL project has fundamentally shifted our understanding of shale reactivity. Knowledge about active reaction networks and the chemical and kinetic factors that control them, obtained from this study, provides a needed scientific foundation to understand and predict the geochemical evolution of shale reservoirs. The findings from this study are being published in leading scientific journals and presented at (inter-)national scientific meetings to ensure that this knowledge is disseminated within the geoscience community.

A renewal project, starting in FY 2017, will build upon these molecular- and pore-scale findings by developing experimental and modeling contexts that scale across shale matrix-fracture interfaces to fracture- and reservoir scales. This new activity will substantially expand the scope and impact of the initial 2 year program by allowing us to understand how fine-scale processes control large-scale shale-fluid behavior and the long-term production of unconventional natural gas and oil.

APPENDIX A. Deliverables

Publications

Anna L. Harrison, Adam D. Jew, Megan K. Dustin, Dana L. Thomas, Claresta M. Joe-Wong, John R. Bargar, Natalie Johnson, Gordon E. Brown Jr., and Katharine Maher. Element release and reaction-induced porosity alteration during shale-hydraulic fracturing fluid interactions. *Applied Geochemistry* (in review).

Adam D. Jew, Megan K. Dustin, Anna L. Harrison, Claresta M. Joe-Wong, Dana L. Thomas, Katharine Maher, Gordon E. Brown Jr., and John R. Bargar. Impact of Organics and Carbonates on the Oxidation and Precipitation of Iron during Hydraulic Fracturing of Shale. *Energy and Fuels* (in review).

Andrew M. Kiss, A. D. Jew, C. Joe-Wong, K. M. Maher, Y. Liu, G. E. Brown, and J. Bargar (2015) Synchrotron-based transmission X-ray microscopy for improved extraction in shale during hydraulic fracturing, SPIE Optical Engineering + Applications, 95920O.

*Oral presentations at scientific meetings (†invited, *presenting author)*

Andrew M. Kiss*, Arjun H. Kohli, Anna L. Harrison, Adam D. Jew, Jae-Hong Lim, Yijin Liu, Katherine M. Maher, Mar D. Zoback, Gordon E. Brown, and John R. Bargar (2016) 4D synchrotron X-ray imaging to understand porosity development in shales during exposure to hydraulic fracturing fluid. Presented at the American Geophysical Union Fall Meeting, Symposium H11E, Fluid-Rock Interactions Controlling Structure, Flow, and Transport in the Subsurface I, San Francisco, USA, December 12-16.

Anna L. Harrison, Katharine Maher*, Adam D. Jew, Megan K. Dustin, Andrew M. Kiss, Arjun H. Kohli, Dana L. Thomas, Claresta Joe-Wong, Gordon E. Brown Jr., and John R. Bargar (2016) The Impact of Mineralogy on the Geochemical Alteration of Shales During Hydraulic Fracturing Operations. Presented at the American Geophysical Union Fall Meeting, Symposium H21J, Fluid-Rock Interactions Controlling Structure, Flow, and Transport in the Subsurface IV, San Francisco, USA, December 12-16.

Adam D. Jew*, Megan K. Dustin, Anna L. Harrison, Claresta Joe-Wong, Dana L. Thomas, Katharine Maher, Gordon E. Brown Jr., and John R. Bargar (2016) The Importance of pH, Oxygen, and Bitumen on the Oxidation and Precipitation of Fe(III)-(oxy)hydroxides during Hydraulic Fracturing of Oil/Gas Shales. Presented at the American Geophysical Union Fall Meeting, Symposium H21J, Fluid-Rock Interactions Controlling Structure, Flow, and Transport in the Subsurface IV, San Francisco, USA, December 12-16.

Anna L. Harrison, Adam D. Jew, Megan K. Dustin, Claresta Joe-Wong, Dana L. Thomas, Katharine Maher*, Gordon E. Brown Jr., and John R. Bargar (2016) Physical and chemical alteration of shales during hydraulic fracturing. Presented at the 2016 Goldschmidt Conference, Yokohama, Japan. 29 June.

†John R. Bargar*, Gordon E. Brown, Jr., Megan K. Dustin, Anna L. Harrison, Adam D. Jew, Andy F. Kiss, C.M. Joe-Wong, Katharine Maher, and Yijin Liu (2016) Geochemistry of fluid-shale reactions at pore to fracture scales. Presented at the 252nd ACS National Meeting, Symposium on Geochemistry of the Subsurface: CO2 Sequestration,

Unconventional Oil & Gas Extraction, Geothermal Reservoirs & Radioactive Waste Disposal, Philadelpha, PA, August 21.

†John R. Bargar*, Gordon E. Brown, Jr., Megan K. Dustin, Anna L. Harrison, Adam D. Jew, Andy F. Kiss, C.M. Joe-Wong, Katharine Maher, and Yijin Liu (2016) Chemical control of fluid flow and contaminant release in shale microfractures. Presented at the Mastering the Subsurface Through Technology, Innovation and Collaboration: Carbon Storage and Oil and Natural Gas Technologies Review Meeting, Philadelpha, PA, August 18.

†John R. Bargar*, Gordon E. Brown, Jr., Megan K. Dustin, Anna L. Harrison, Adam D. Jew, Andy F. Kiss, C.M. Joe-Wong, Katharine Maher, and Yijin Liu (2016) Chemical control of fluid flow and contaminant release in shale microfractures. Presented at the NETL Shale Research Portfolio Collaboration Meeting, Los Alamos, NM, July 14.

Anna L. Harrison, Adam D. Jew, Megan K. Dustin, Claresta Joe-Wong, Dana L. Thomas, Katharine Maher*, Gordon E. Brown Jr., and John R. Bargar (2016) Physical and chemical alteration of shales during hydraulic fracturing. Presented at the 2016 Goldschmidt Conference, Yokohama, Japan. 29 June.

†Megan K. Dustin*, Adam D. Jew, Anna L. Harrison, Claresta Joe-Wong, Dana L. Thomas, Katharine Maher, Gordon E. Brown Jr., and John R. Bargar (2016) Effects of Fluid-Rock Interactions on Shale Transport Properties. Stanford Center for Secure Carbon Storage Research Seminar, Stanford, USA, May 26.

†Anna L. Harrison*, Adam D. Jew, Megan K. Dustin, Claresta Joe-Wong, Dana L. Thomas, Katharine Maher, Gordon E. Brown Jr., and John R. Bargar (2015) A Geochemical Framework for Evaluating Shale-Hydraulic Fracture Fluid Interactions. Stanford Center for Secure Carbon Storage Research Seminar, Stanford, USA, October 21.

†John R. Bargar*, Gordon E. Brown, Jr., Megan K. Dustin, Anna L. Harrison, Adam D. Jew, C.M. Joe-Wong, and Katharine Maher (2015) Geochemical control of shale fracture and matrix permeability. Shales without Scales Workshop, Santa Fe, USA, June 10.

†John R. Bargar*, Gordon E. Brown, Jr., Megan K. Dustin, Anna L. Harrison, Adam D. Jew, C.M. Joe-Wong, and Katharine Maher (2015) Geochemical control of shale fracture and matrix permeability. Baker Hughes Incorporated, Tomball, USA, July 14.

Conference poster presentations (*presenting author)

Megan K. Dustin*, Adam D. Jew, Anna L. Harrison, Claresta Joe-Wong, Dana L. Thomas, Katharine Maher, Gordon E. Brown Jr., and John R. Bargar (2015) Kerogen-Hydraulic Fracture Fluid Interactions: Reactivity and Contaminant Release. American Geophysical Union Fall Meeting, San Francisco, USA, December 14-18.

Anna L. Harrison*, Adam D. Jew, Megan K. Dustin, Claresta Joe-Wong, Dana L. Thomas, Katharine Maher, Gordon E. Brown Jr., and John R. Bargar (2015) A Geochemical Framework for Evaluating Shale-Hydraulic Fracture Fluid Interactions. American Geophysical Union Fall Meeting, San Francisco, USA, December 14-18.

Adam D. Jew*, Claresta Joe-Wong, Anna L. Harrison, Dana L. Thomas, Megan K. Dustin, Gordon E. Brown Jr., Katharine Maher, and John R. Bargar (2015) Iron Release and

Precipitation in Hydraulic Fracturing Systems. American Geophysical Union Fall Meeting, San Francisco, USA, December 14-18.

Claresta Joe-Wong*, Anna L. Harrison, Dana L. Thomas, Megan K. Dustin, Adam D. Jew, Gordon E. Brown Jr., Katharine Maher, and John R. Bargar (2015) Coupled mineral dissolution and precipitation reactions in shale-hydraulic fracturing fluid systems. American Geophysical Union Fall Meeting, San Francisco, USA, December 14-18.

Megan K. Dustin*, Adam D. Jew, Anna L. Harrison, Claresta Joe-Wong, Dana L. Thomas, Katharine Maher, Gordon E. Brown Jr., and John R. Bargar (2015) Kerogen-Hydraulic Fracture Fluid Interactions: Reactivity and Contaminant Release. Stanford Synchrotron Radiation Lightsource 2015 User's Meeting, Stanford, USA, Oct 7-9.

Anna L. Harrison*, Adam D. Jew, Megan K. Dustin, Claresta Joe-Wong, Dana L. Thomas, Katharine Maher, Gordon E. Brown Jr., and John R. Bargar (2015) A Geochemical Framework for Evaluating Shale-Hydraulic Fracture Fluid Interactions. Stanford Synchrotron Radiation Lightsource 2015 User's Meeting, Stanford, USA, Oct 7-9.

Megan K. Dustin*, Adam D. Jew, Anna L. Harrison, Dana L. Thomas, Claresta Joe-Wong, Kate Maher, Gordon E. Brown, Jr., John R. Bargar. (2016) Alteration of kerogen during reaction with hydraulic fracturing solution. Stanford Synchrotron Radiation Lightsource 2016 User's Meeting, Stanford, USA, Oct. 5-8.

Adam D. Jew*, Megan K. Dustin, Anna L. Harrison, Claresta Joe-Wong, Dana Thomas, Kate Maher, Gordon Brown, Jr., John Bargar. (2016) The importance of pH, oxygen, and bitumen on the oxidation and precipitation of Fe(III)-(oxy)hydroxides during hydraulic fracturing of oil/gas shales. Stanford Synchrotron Radiation Lightsource 2016 User's Meeting, Stanford, USA, Oct. 5-8.

Megan K. Dustin*, Adam D. Jew, Anna L. Harrison, Dana L. Thomas, Claresta Joe-Wong, Kate Maher, Gordon E. Brown, Jr., John R. Bargar. (2016) Alteration of kerogen during reaction with hydraulic fracturing solution. Stanford Natural Gas Initiative Affiliates Meeting, Oct. 12.

Adam D. Jew*, Megan K. Dustin, Anna L. Harrison, Claresta Joe-Wong, Dana Thomas, Kate Maher, Gordon Brown, Jr., John Bargar. (2016) The importance of pH, oxygen, and bitumen on the oxidation and precipitation of Fe(III)-(oxy)hydroxides during hydraulic fracturing of oil/gas shales. Stanford Natural Gas Initiative Affiliates Meeting, Oct. 12.

Anna L. Harrison*, Adam D. Jew, Megan K. Dustin, Claresta Joe-Wong, Dana L. Thomas, Katharine Maher, Gordon E. Brown Jr., Markus Bill, Mark Conrad, David, Cercone, and John R. Bargar. (2016) A geochemical framework for evaluating shale-hydraulic fracture fluid interactions. Stanford Natural Gas Initiative Affiliates Meeting, Oct. 12.